LA-UR-15-26303 (Accepted Manuscript)

Multi-scale predictions of massive conifer mortality due to chronic temperature rise

Mcdowell, Nathan Gabriel; Sevanto, Sanna Annika; Xu, Chonggang; Williams, Park; Rauscher, Sara; Koven, Charles; Domec, JC; Mackay, Scott; Fisher, Rosie; Pockman, William; Dickman, Lee Thoresen; Pangle, Rob; Limousin, JM; Ogee, Jerome; Allen, Craig; Jiang, X; Muss, Jordan; Breshears, David

To be published in: Nature Climate Change

DOI to publisher's version: 10.1038/nclimate2873

Permalink to record: http://permalink.lanl.gov/object/view?what=info:lanl-repo/lareport/LA-UR-15-26303

Multi-scale predictions of massive conifer mortality due to chronic temperature rise

N.G. McDowell[1*], A.P. Williams[1,2], C. Xu[1], W.T. Pockman[3], L.T. Dickman[1], S. Sevanto[1], R. Pangle[3], J. Limousin[3], J. Plaut[3], D. Scott Mackay[4], J. Ogee[5], J.C. Domec[5,6], C.D. Allen[7], R.A. Fisher[8], X. Jiang[8], J.D. Muss[1], D.D. Breshears[9], S. A. Rauscher[10], C. Koven[11]

[1]Earth and Environmental Sciences Division, MS-J495, Los Alamos National Lab, Los Alamos, NM 87545, USA. Correspondence: mcdowell@lanl.gov

[*]Author for correspondence

[2]Lamont-Doherty Earth Observatory, Columbia University, Palisades, NY 10964

[3]Biology Department, University of New Mexico, Albuquerque, NM, USA

[4] Department of Geography, University at Buffalo, Buffalo, NY, USA

[5]UMR 1391 ISPA, INRA-Bordeaux Sciences Agro, Villenave d'Ornon, 33140 France

[6]Nicholas School of the Environment, Duke University, Durham, NC 27708, USA

[7]U.S. Geological Survey, Fort Collins Science Center, Jemez Mountains Field Station, Los Alamos, NM 87544 USA.

[8]National Center for Atmospheric Research. Boulder, Colorado, 80305 USA.

[9]School of Natural Resources and the Environment, and Department of Ecology and Evolutionary Biology, University of Arizona, Tucson, AZ, 85721, USA

[10]Department of Geography, University of Delaware, Newark, DE, 19716

[11]Earth Sciences Division, Lawrence Berkeley National Lab, 1 Cyclotron Rd., Berkeley, CA 94720

Submission as a Letter to Nature Climate Change

Introduction: Global temperature rise and extremes accompanying drought threaten forests[1,2] and their associated climatic feedbacks[3,4]. Our ability to accurately simulate drought-induced forest impacts remains highly uncertain[5-6] in part due to our failure to integrate physiological measurements, regional-scale models, and dynamic global vegetation models (DGVMs). Here we show consistent predictions of widespread mortality of needleleaf evergreen trees (NET) within Southwest USA by 2100 using state-of-the-art models evaluated against empirical datasets, whilst the less mechanistic DGVMs lacked sufficient vegetation resolution to predict this regional change but nonetheless predicted $\geq$50% loss of northern hemisphere NET by 2100. Experimentally, dominant Southwest USA NET species died when they fell below predawn water potential (Ψ_{pd}) thresholds (April-August mean) beyond which photosynthesis, hydraulic and stomatal conductance, and carbohydrate availability approached zero. The evaluated regional models accurately predicted NET Ψ_{pd}, and 91% of predictions (10 out of 11) exceeded mortality thresholds within the 21st century due to temperature rise. The independent DGVMs predicted $\geq$50% loss of northern hemisphere NET by 2100, consistent with the NET findings for Southwest USA. Notably, the global models underestimated future mortality within Southwest USA, highlighting that predictions of future mortality within global models may be underestimates. Taken together, the validated regional predictions and the global simulations predict widespread conifer loss in coming decades under projected global warming.

Forest mortality has been widely documented in recent years[1,2,7,8] and has accelerated in concert with rising CO_2 and temperature ([2,7]; Fig. 1A, SI 1). The terrestrial carbon sink could be severely diminished over the next century if this acceleration of tree mortality continues with warming and increased extreme drought events[5,9], causing a positive feedback on global warming[3,10]. Unfortunately, predictions of the terrestrial carbon sink vary dramatically across models (e.g. [5]) in part because the mechanisms of tree death are still poorly understood[6] thus forecasts remain largely speculative.

Here we demonstrate that predawn plant water potential (Ψ_{pd}), through its impact on canopy scale stomatal conductance (G_s) and regulation of carbon and water balance is a key predictive element to mechanistically represent vegetation mortality. We extend this analysis to include multiple process-based and empirical models to investigate the likelihood of future mortality of needleleaf evergreen trees (NET) in Southwest USA. We then compare these results to those from the dynamic global vegetation models (DGVMs) from the CMIP5 (Coupled Model Intercomparison Project, Phase 5) to examine if completely independent simulations provide similar predictions for the NET biome as predicted for Southwest USA. This last step further allows comparison within the Southwest USA of the un-evaluated and less mechanistic DGVMs predictions against the evaluated simulations of the regional models.

Plants must balance multiple demands upon stomatal control during drought: severe water potential declines promote hydraulic failure[11], while G_s reductions limit this decline and minimize the risk of hydraulic failure but thus inhibit CO_2 diffusion into leaves[12]. G_s decline *per se* does not induce mortality, but theory and evidence point to drought-induced declines in hydraulic function and photosynthesis (via G_s decline) as the primary drivers of death because of their downstream impacts leading to carbon starvation, hydraulic failure, and biotic attack,

74 particularly if G_s is low for long durations[6,13-17]. The G_s response to drought varies across the
75 isohydry-anisohydry continuum of hydraulic strategies[18] (Fig. 1B, SI 2). Across this continuum
76 of hydraulic strategies, G_s declines with decreasing soil water potential (Ψ_s) or leaf water
77 potential (Ψ_l), decreasing hydraulic conductance (k), and increasing vapor pressure deficit (D)
78 ([19], Fig. 1B):
79
80 $$G_s = \frac{k(\Psi_s - \Psi_l)c}{D} \quad (1).$$
81
82 Equation (1), where c is a coefficient representing air and water thermodynamic properties, is a
83 simplified model (SI3) that illustrates the dependence of G_s, and therefore photosynthesis, on
84 drought induced declines in k (which declines along the continuum of hydraulic failure during
85 drought), Ψ_s, and increasing D (the atmospheric driving force for transpiration). Equation (1)
86 has been validated in numerous studies (SI3), and assumes steady-state conditions and adequate
87 coupling between the canopy and the atmosphere (reviewed in SI3 and in[17]). Because survival
88 depends on sustained maintenance of a net positive G_s[6,12-17], equation (1) also suggests mortality
89 may increase when drought causes a sustained decrease in Ψ_s or k, and an increase in D (Fig.
90 1B). Rising D is potentially the largest threat to survival associated with climate change because
91 global temperature rise is driving a chronic rise in D[20].
92 We first combined observational and experimental datasets with models (using both
93 published and unpublished data and simulations[13]) to examine the likelihood of future mortality
94 and survival for piñon pine and juniper trees (*Pinus edulis and Juniperus monosperma*) in
95 Southwest USA. In a field experiment, we removed ~48% of ambient rainfall from three 1600
96 m^2 plots for five years in a piñon-juniper woodland in central New Mexico, USA (SI 4). We

made measurements of Ψ_{pd}, G_s and other variables critical to plant survival during drought[6]. Across the three drought plots, the mature (> 100 years old) piñon pine experienced ~80% whole-tree mortality; trees with April-August mean (growing season[20]) Ψ_{pd} averaging -2.4 MPa or lower all died (Fig. 2A, SI 4). Crown dieback of juniper started after a continuous April-August period with Ψ_{pd} below -5.3 MPa, resulting in ~50% canopy loss and approximately 25% whole-tree mortality. The Ψ_{pd} value associated with mortality was consistent with the Ψ value associated with zero G_s and zero photosynthesis (Ψ_{A0}) for each species (Fig. 2B, 2C, see SI5 for all regression statistics from Fig 2). Consistent exceedance of Ψ_{pd} below Ψ_{A0} during April-August (i.e. maintaining negative Ψ_{A0} values) resulted in downstream consequences on the physiology of both species, including severe levels of hydraulic failure (percentage loss of whole-tree conductance; Fig. 2D), near-zero whole-tree k (Fig. 2E), and reductions in foliar starch (Fig. 2F). Extreme values in Figure (2B-F) were consistent with the Ψ_{pd} mortality thresholds for each species (Fig. 2A). Additionally, formation of resin ducts for defense against biotic attack declined to nearly zero in the pine trees that died but remained high for those that survived[21]. Therefore, all potential mechanisms of mortality reached similarly critical values at or before species-specific Ψ_{A0} values (Fig. 2; SI6).

The Ψ_{pd} mortality thresholds identified from the drought experiment (Fig. 2) validated well against the world's longest continuous Ψ_{pd} record, also for piñon pine and juniper trees in New Mexico (an extension of [22,23]; SI Fig. 1A). Using this long-term dataset, we assessed if precipitation and D predicted by the CMIP5 multi-model ensembles could be used to infer our long-term Ψ_{pd} observations (1992-2013). Observed annual precipitation and D together explain 70 and 80% of the annual variation in growing-season mean Ψ_{pd} for pine and juniper, respectively, at the long-term observational site (SI Fig. 1). An independent test against the

120 drought manipulation site (Fig. 2) also produced a strong predictive relationship for both species
121 (SI Figs. 1,2).

122 The strength of empirical models (e.g. equations SI 2,3) is that they reflect the
123 observations without need to simulate processes; however, they may not capture future non-
124 linearity — in this case, responses to a future world with higher temperature, *D*, and CO_2. We
125 investigated simulations by the process-based models TREES, MuSICA and ED(X) that account
126 for non-linear effects of changes in these variables (see SI7 and SI Fig. 3). After model tuning
127 (SI6) each model simulated each species Ψ_{pd} as accurately as the empirical model (SI Fig. 2).

128 The "business-as-usual" greenhouse gas emissions scenario (RCP 8.5) from CMIP5
129 suggests that by 2100 AD, precipitation will decrease by 10% and *D* will increase by 33% in
130 Southwest USA (Fig. 3A, B). Using these climate projections to drive the empirical and process-
131 based models resulted in relatively consistent predictions of declining Ψ_{pd} over time for both
132 piñon and juniper (SI Figs. 4,5), falling below the Ψ_{A0} threshold for both species by 2020-2060
133 (Fig. 3C, SI Fig. 4). This outcome is delayed by approximately one decade when RCP 4.5, a
134 more optimistic greenhouse gas reductions scenario, is used (SI Fig. 6). These predictions are
135 consistent with NET losses for a tree-ring-based forest drought stress model[20] and for both
136 Southwest and Northwest USA from the Community Earth System Model (CESM[24]; Fig. 3C).
137 Averaging all models shown in Figure (3C) suggests that 72% of the regions NET forests will
138 experience mortality by 2050, with nearly 100% mortality of Southwest USA forests by 2100.

139 The simulations shown in Figure (3C) suggest that Southwest NET species, even the
140 particularly drought-tolerant piñon pine and juniper trees, are likely to experience widespread
141 mortality before 2100. Substantial documented piñon mortality in the early 2000s[1,20,22,23] and
142 widespread observations of recent juniper mortality (SI Fig. 1B) in Southwest USA are

143 consistent with this result, despite juniper's reputation as being this region's most drought
144 tolerant conifer[23]. We note that all predictions shown in Figure (3C) are independent except for
145 their use of CMIP5 ensemble climate forecasts. ED(X), the most conservative model, predicted
146 two less severe trends (Fig. 3C). First, ED(X) indicated that juniper could survive well into the
147 22nd century (Figure 3C) due in part to juniper's particularly low vulnerability to cavitation,
148 which is rare amongst the NET plant functional type[25]. Second, ED(X) was run for 72 one-
149 degree grid cells over Southwest USA (Fig. 3D), predicting that mortality will occur primarily in
150 warmer southern locations. ED(X) results suggest that temperature is the primary driver of
151 mortality through increasing *D* (SI Figure 7). Given the importance of temperature to tree
152 survival, future forest management may take advantage of potential refugia in cooler landscape
153 locations and planting of warm-adapted genotypes.
154 We placed our results for the Southwest USA into a global context through comparison to
155 independent NET simulations for the Northern Hemisphere from four DGVMs that were run
156 with dynamic vegetation enabled (SI 8). This comparison allowed building of confidence in our
157 predictions if the independent, non-evaluated DGVMs provided similar results for the NET
158 biome at the global scale as those from the evaluated regional process models, and this further
159 allowed direct regional comparison of the DGVMs to the evaluated and more detailed process
160 model predictions for Southwest USA. The first three DGVM simulations are Earth System
161 Models (ESMs) from the CMIP5 archive that have interacting land-atmosphere-ocean dynamics,
162 and are entirely independent of those shown in Figure (3C), thus allowing us to examine the
163 robustness of our predictions of NET loss under alternative modeled drivers and assumptions for
164 climates outside the Southwest USA. These ESMs do not utilize the Ψ_{pd} thresholds identified in
165 this analysis because such extrapolation of a model developed in Southwest USA to wetter,

166 cooler regions of the NET biome, with other species and climate, would likely be inaccurate.
167 These ESMs instead rely on the climate envelope and low growth thresholds typical of DGVMs[6]
168 making them largely independent of the Southwest USA simulations shown in Figure (3C). All
169 three ESMs simulated large NET losses throughout the temperate and southern boreal regions
170 although NET forest gains in MPI outweighed the losses (-14.5 million km^2 on average; Fig. 4A-
171 C; see SI 9 for calculation explanation). Our fourth DGVM (CESM) simulated NET
172 distributions through 2100 using coupled land-atmosphere dynamics forced by eight different sea
173 surface temperature (SST) scenarios from fully coupled GCMs provided by CMIP3[26]. SST
174 patterns play an important role in shaping how precipitation may change in a warmer world
175 (e.g.[27]); therefore the use of different SSTs generates a range of potential future climate scenarios
176 within the same model framework. The eight simulations agreed that at least 50% of the NET
177 plant functional type could be lost within the northern hemisphere by 2100, as indicated by the
178 red swath across the temperate zone (Fig. 4D). Therefore, all four DGVMs and the more
179 rigorous analysis for Southwest USA predict potential large scale NET mortality despite
180 covering different regions and utilizing different mortality algorithms.
181 Despite the consistent predictions of widespread NET mortality highlighted in both Fig.
182 3C and Fig. 4A-D, a notable discrepancy emerges through comparison of the DGVMs
183 predictions of mortality in Southwest USA (Fig. 4E-H) to those of the validated ED(X) model
184 (Figure 3D). This may be caused by the lack of NET coverage in Southwest USA as prescribed
185 by the DGVMs, by the DGVMs lumping of NET species into one plant functional type, and by
186 their simplistic climate envelope and low-growth mortality thresholds. Assuming that the
187 accuracy of the predictions in Fig. (3C) is better than that of the DGVMs (because the models in
188 Fig. 3C were developed and validated for this region), the discrepancy thus suggests that the

189 DGVMs may be too conservative in their predictions of NET mortality, at least for Southwest
190 USA, and provides motivation to improve the realism and evaluate the performance of future
191 DGVM simulations. We note two additional caveats to the results shown in Fig. (4). First, global
192 DGVM predictions have never been validated, so while their predictions represent the state-of-
193 the-art in global simulations, we cannot absolutely trust their outcomes to be realistic. Second,
194 there are multiple processes not included in the models that could cause: (1) overestimates of
195 future mortality, e.g., by not accounting for acclimation, adaptation, and islands of refugia (such
196 as those associated with beneficial topographic settings)[28]; or conversely (2) underestimate future
197 mortality by not including processes such as acceleration of insect population dynamics,
198 increases in frequency and severity of wildfires, or failure of seedling recruitment[6,20].
199 The general agreement of rising mortality rates of the NET biome located within
200 Southwest USA (Fig. 3), western and boreal North America (Fig. 1A[2,7]), and the northern
201 hemisphere (Fig. 4), based on models and datasets with very different sets of assumptions and
202 mechanisms, suggests a high likelihood that widespread mortality of NET forests will occur by
203 2100. The recently accelerating NET mortality rates are associated with warming (e.g. SI Fig. 7;
204 and see[2,7,29]). The rise in juniper mortality likelihood has alarming implications for conifers in
205 general because juniper historically experienced far less mortality than other conifers during
206 droughts[1,13,22,23]. The consequences of such broad-scale change in forest cover are substantial,
207 including massive transfer of carbon to a decomposable pool[10] and changes in the surface energy
208 budget[3,4]. The carbon consequences of tree mortality across the NET biome averaged 10 Pg C
209 for the models shown in Fig. (4A-C), which is equivalent to predicted boreal carbon loss over the
210 next century[30]. The projections are more optimistic for the far northern latitudes (Fig. 4);

however, these boreal systems have lower carbon fluxes than the majority of temperate zone forests.

These simulations of climate-induced vegetation change (Fig. 3C) are among the most rigorously tested by both experimental and observational data sets of physiological conditions associated with tree mortality. The ensemble analyses in this study consistently highlight vulnerability to collapse of the NET biome across many parts of the globe in coming decades, driven by warming temperatures and associated drought stress. Such rapid and extensive forest losses are likely to have profound impacts on carbon storage, climate forcing, and ecosystem services[31].

References and Notes

1. C. D. Allen *et al.*, A global overview of drought and heat-induced tree mortality reveals emerging climate change risks for forests. *Forest Ecology and Management* **259**, 660-684 (2010).

2. S. Peng *et al*., A drought-induced pervasive increase in tree mortality across Canada's boreal forest*. Nature Climate Change* **1**, 467-471 (2011).

3. G. B. Bonan, Forests and climate change: Forcings, feedbacks, and the climate benefits of forests. *Science* **320**, 1444-1449 (2008).

4. H. Maness, P. J. Kushner, I. Fung, Summertime climate response to mountain pine beetle disturbance in British Columbia. *Nature Geoscience* **6**, 65-70 (2012).

5. P. Friedlingstein *et al*. Uncertainties in CMIP5 Climate Projections due to Carbon Cycle Feedbacks. *Journal of Climate* **27**, no. 2 (2014).

6. N. G. McDowell *et al.*, Interdependence of mechanisms underlying climate-driven vegetation mortality. *Trends in Ecology and Evolution* **26**, 523-532 (2011).

7. P. J. Van Mantgem *et al.*, Widespread increase of tree mortality rates in the western United States. *Science* **323**, 521-524 (2009).

8. O. L. Phillips *et al.*, Drought sensitivity of the Amazon rainforest. *Science* **323**, 1344-47 (2009).

9. M. Reichstein *et al.*, Climate extremes and the carbon cycle. *Nature* **500**, 287-295 (2013).

10. W. A. Kurz *et al.*, Mountain pine beetle and forest carbon feedback to climate change. *Nature* **452**, 987-990 (2008).

11. J. Plaut, E.A. *et al.*, Hydraulic limits on water use under experimental drought in a piñon-juniper woodland. *Plant, Cell and Environment* **35**, 1601-1617 (2012).

12. I. R. Cowan, T. J. Givnish, Economics of carbon fixation in higher plants, in *On the economy of plant form and function* (Cambridge University Press, Cambridge, 1986), pp. 133-170.

13. N. G. McDowell *et al.*, Evaluating theories of drought-induced vegetation mortality using a multi-model-experiment framework. *New Phytologist* **200**, 304-321 (2013).

14. P.J. Mitchell *et al.*, Drought response strategies define the relative contributions of hydraulic dysfunction and carbohydrate depletion during tree mortality. *New Phytologist* **197**, 862-872 (2013).

15. R. Poyatos *et al.* Drought-induced defoliation and long periods of near-zero gas exchange play a key role in accentuating metabolic decline of Scots pine. *New Phytologist* **200**, 388-401 (2013).

16. S. Sevanto *et al.* How do trees die? A test of the hydraulic failure and carbon starvation hypotheses. *Plant, Cell and Environment* **37**, 153-161 (2013).

17. N. McDowell, C. Allen. Darcy's law predicts widespread forest loss due to climate warming. *Nature Climate Change* in press.

18. J. Martínez-Vilalta *et al.* A new look at water transport regulation in plants. *New Phytologist* **204**, 105-115 (2014).

19. D. Whitehead, P. G. Jarvis, in *Water deficits and growth,* T.T. Kozlowski, Ed. (Academic Press, New York, 1981), vol. 6, pp. 49-152.

20. A. P. Williams *et al.*, Temperature as a potent driver of regional forest drought stress and tree mortality. *Nature Climate Change* **3**, 292-297 (2013).

21. M. L. Gaylord *et al.*, Drought predisposes piñon-juniper woodlands. *New Phytologist* **198**, 567-568 (2012).

22. N. G. McDowell *et al.*, Mechanisms of plant survival and mortality during drought: why do some plants survive while others succumb? *New Phytologist* **178**, 719-739 (2008).

23. D. D. Breshears *et al.*, Tree die-off in response to global-change-type drought: mortality insights from a decade of plant water potential measurements. *Frontiers in Ecology and Environment* **7**, 185-189 (2009).

24. X. Jiang *et al*., Projected future changes in vegetation in western North America in the 21st century. *Journal of Climate*, 10.1174/JCLI-D-12-00430.1 (2013).

25. B. Choat *et al.*, Global convergence in the vulnerability of forests to drought. *Nature* **491**, 752-755 (2012).

26. Gerald A. Meehl *et al.*, The WCRP CMIP3 multimodel dataset: A new era in climate change research. *Bulletin of the American Meteorological Society* **88**, 1383-1394 (2007).

27. S.A. Rauscher, F. Kucharski, D. B. Enfield, The role of regional SST warming variations in the drying of meso-America in future climate projections. *J. Climate*, **24**, 2003–2016 (2011).

279 28. Lloret, Francisco, Adrian Escudero, José María Iriondo, Jordi Martínez-Vilalta, and
280 Fernando Valladares. Extreme climatic events and vegetation: the role of stabilizing processes.
281 *Global Change Biology* **18**, no. 3, 797-805 (2012).

282 29. Carnicer, Jofre, Marta Coll, Miquel Ninyerola, Xavier Pons, Gerardo Sánchez, and Josep
283 Peñuelas. Widespread crown condition decline, food web disruption, and amplified tree mortality
284 with increased climate change-type drought. *Proceedings of the National Academy of Sciences*
285 **108**, no. 4 (2011): 1474-1478.

286 30. C.D. Koven. Boreal carbon loss due to poleward shift in low-carbon ecosystems. *Nature*
287 *Geoscience,* **6**, 452-456 (2013).

288 31. Settele, J., R. Scholes, R. Betts, S. Bunn, P. Leadley, D. Nepstad, J.T. Overpeck, and M.A.
289 Taboada, 2014: Terrestrial and inland water systems. In: *Climate Change 2014: Impacts,*
290 *Adaptation, and Vulnerability. Part A: Global and Sectoral Aspects. Contribution of Working*
291 *Group II to the Fifth Assessment Report of the Intergovernmental Panel on Climate Change*
292 Field, C.B., V.R. Barros, D.J. Dokken, K.J. Mach, M.D. Mastrandrea, T.E. Bilir, M. Chatterjee,
293 K.L. Ebi, Y.O. Estrada, R.C. Genova, B. Girma, E.S. Kissel, A.N. Levy, S. MacCracken, P.R.
294 Mastrandrea, and L.L. White (eds.). Cambridge University Press, Cambridge, United Kingdom
295 and New York, NY, USA, pp. 271-359.

296

297

298 **Acknowledgments:** This work was funded by the Department of Energy, Office of Science, Los
299 Alamos National Lab's Lab Directed Research and Development program, by NSF-EAR-
300 0724958 and NSF-EF-1340624, by Department of Agriculture AFRI-NIFA program, by
301 U.S.G.S. Climate and Land Use Program, and by a National Science Foundation grant to the
302 University of New Mexico for Long Term Ecological Research.
303

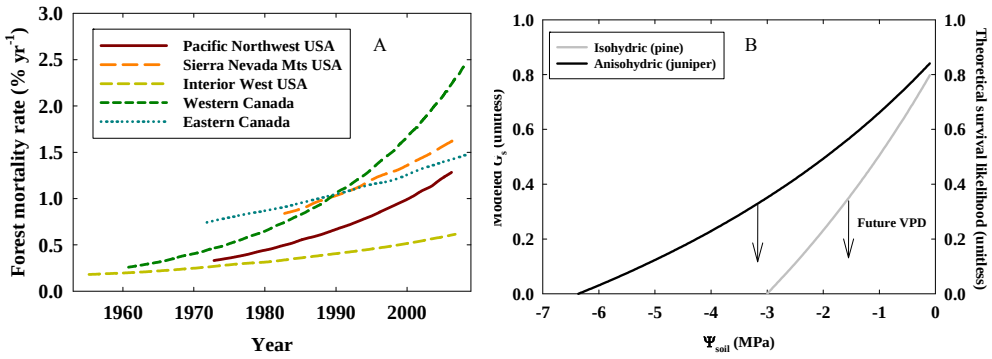

Figure 1A): Reported mortality observations are increasing throughout North America, across a mean annual precipitation range of 202 to 3928 mm yr^{-1} and a mean annual temperature range of -5.7 to 12.0°C ([2,7]). **1B)**: Predictions of stomatal conductance and by inference, survival of relatively isohydric and anisohydric species, in response to decreasing soil water potential. Rising future *D* forces a shift downward in the curves, thereby reducing G_s and survival likelihood.

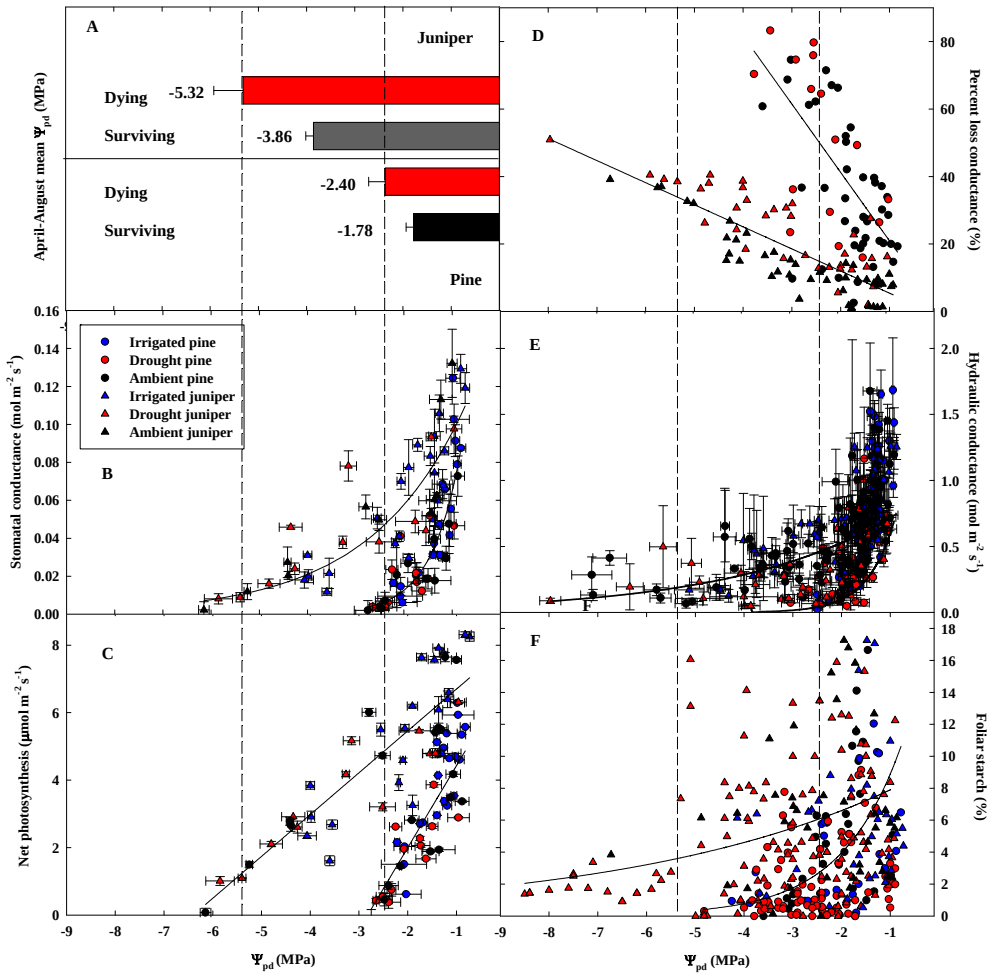

Figure 2A). **Pre-dawn Ψ measurements are strongly correlated with the mechanisms of mortality[6].** Trees that die of each species averaged more negative Ψ from April through August than trees that survived ($p<0.01$ for both species). Vertical lines demark thresholds for pine and juniper. B) Stomatal conductance, C) net photosynthesis, D) modeled whole-tree percent loss of conductance (hydraulic failure), E) measured whole-tree hydraulic conductance, and F) foliar starch all declined with Ψ_{pd} for both species.

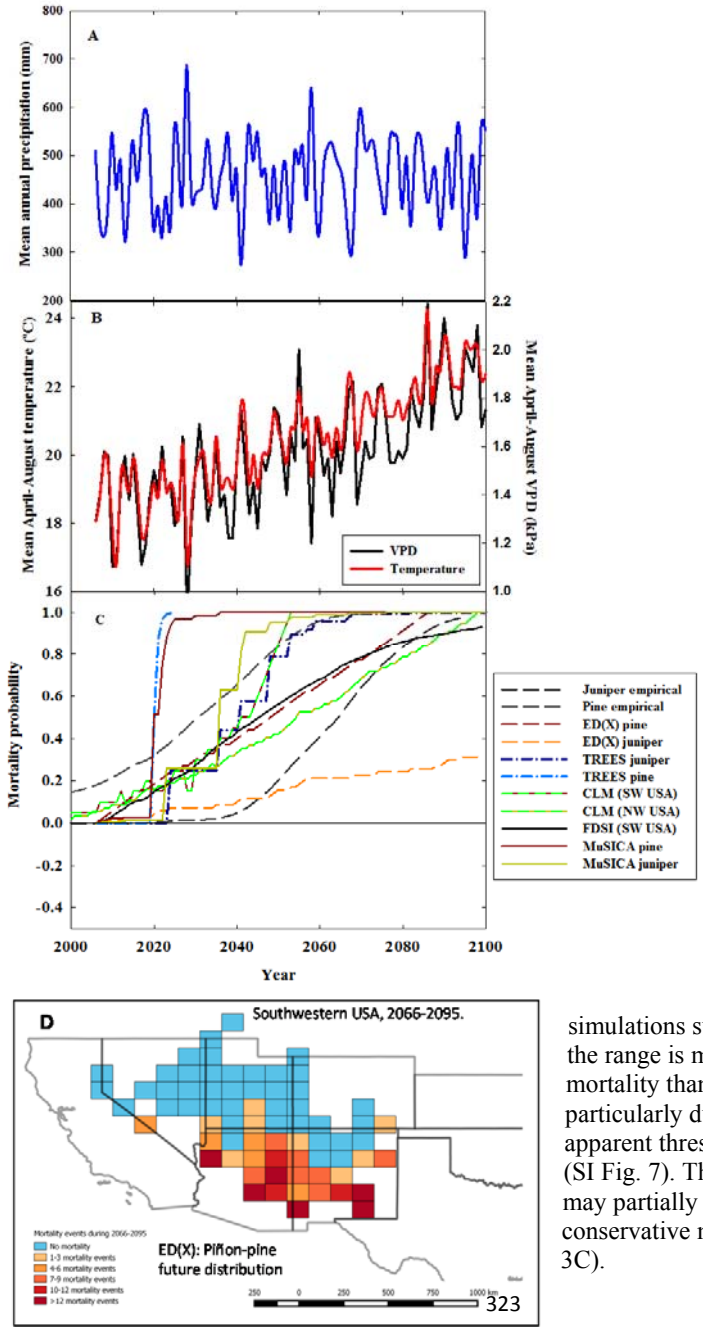

Figure 3. Ensemble forecasts from CMIP5, RCP 8.5, of (A) mean annual precipitation and (B) mean April-August vapor pressure deficit and temperature for the distribution of pine-juniper woodlands in the Southwest USA. (C) Predictions of the probability of future NET mortality events in the Southwest USA based on CMIP5 climate predictions and a variety of modeling approaches. Mortality was a function of simulated Ψ_{pd} exceeding Ψ_{A0} throughout April-August in the empirical model and ED(X), TREES, and MuSICA. CLM[24] used its own mortality algorithms and the Forest Drought Stress Index[20] used a threshold index based on historical observations. (D) ED(X) simulations of the geographic pattern of pine-juniper mortality in the Southwest USA for RCP8.5 for the period 2066-2095. ED(X) simulations suggests the southern half of the range is more likely to experience mortality than the northern half. This is particularly due to warming, with an apparent threshold warming of 1.95 ºC (SI Fig. 7). This regional heterogeneity may partially explain ED(X)'s relatively conservative mortality predictions (Fig. 3C).

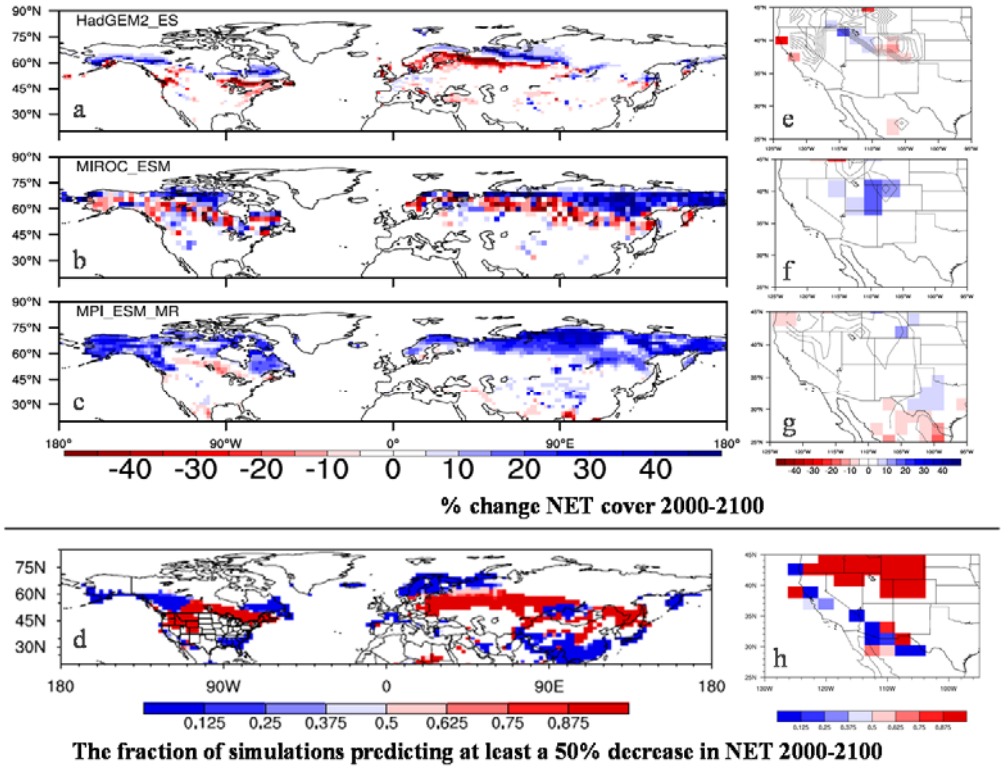

Figure 4. Dynamic global vegetation models predictions of needleleaf evergreen tree (NET) percentage losses between 2000-2100. a) HadGem2, **b**) MIROC_ESM, **c)** MIP_ESMLR, and **d)** CESM. Panels (a-c) show the percent change in NET cover between 2000 and 2100. d) The fraction of eight CESM runs with different sea surface temperature warming patterns, showing the model agreements that at least 50% of NET cover will be lost by 2100. Panels **(e-h)** are blow-ups of panels (a-d) for Southwestern USA, intended for comparison to Figure (3d). (**e-g)** are HadGem2, MIROC_ESM, MIP_ESMLR with no change in representation of the results. Isolines in panels e-g show current NET distributions (in 10% coverage increments). Panels **(d and h)** are presented as the fraction of models that simulate a 50% decrease in NET coverage, to allow more direct comparison to Figure (3d). All simulations are independent of those done for Southwest USA.

Supporting Information for

Convergent predictions of massive conifer mortality due to chronic temperature rise

N.G. McDowell, A.P. Williams, C. Xu, W.T. Pockman, T. Dickman, S. Sevanto, R. Pangle, J. Limousin, J. Plaut, D. Scott Mackay, J. Ogee, J.C. Domec, C.D. Allen, R.A. Fisher, X. Jiang, J. Muss, D.D. Breshears, S. A. Rauscher, C. Koven

Author contributions

[1]Contributed to development of the project and critical important contribution to analysis

[2]Contributed to field work critical to the project

[3]Contributed to model simulations and data analysis critical to the project

[1,2]N.G. McDowell, [1,3]A.P. Williams, [1,3]C. Xu, [1]W.T. Pockman, [2]T. Dickman, [2]S. Sevanto, [2]R. Pangle, [2]J. Limousin, [2]J. Plaut, [1,3]D. Scott Mackay, [1,3]J. Ogee, [1,3]J.C. Domec, [1]C.D. Allen, [1,3]R.A. Fisher, [1,3]X. Jiang, [3]J. Muss, [1,2]D.D. Breshears, [1,3]S. Rauscher, [3]C. Koven

Material and methods. Material provided in the order of presentation in the main text.

SI 1: Figure 1a shows the trend in mortality over time from five regions. These data were previously published in [2,7] and were graciously provided by the lead authors.

SI 2: Figure 1b shows predictions of stomatal conductance from equation (1) using a range of soil water potentials and an assumed vapor pressure deficit of 1 kPa, with anisohydric species water potential gradient declining with soil water potential at 50% the rate of the isohydric species. Anisohydric species are rare amongst NET species, with juniper being amongst the most widespread and drought tolerant. Pines, in contrast, are relatively isohydric (for example [20]).

SI 3: Equation (1) is a fundamental tenet of plant hydraulic theory and has been validated in numerous studies. Most importantly, it has been validated with high rigor and accuracy in field studies (the scale of interest to this study) by Whitehead et al 1984, Whitehead 1998, Oren et al. 1999, McDowell et al. 2006, 2008 and Phillips et al. 2002. Equation (1) assumes that vegetation tends toward space-filling relationships (West et al. 1999) that optimize carbon gain for water loss (Cowan and Givnish 1986). Papers in support of Darcy's law derived for trees (equation 1):

McDowell NG, White S, Pockman WT. Transpiration and stomatal conductance across a steep climate gradient in the southern Rocky Mountains. *Ecohydrology*, **1**:193-204. (2008)

McDowell NG, Adams HA, Bailey JD, Hess M, Kolb TE. Homeostatic maintenance of ponderosa pine gas exchange in response to stand density changes. Ecol Appl **16**(3):1164-1182 (2006)

Oren R, Sperry JS, Katul GG, Pataki DE, Ewers BE, Phillips N, Schäfer K VR. Survey and synthesis of intra- and interspecific variation in stomatal sensitivity to vapour pressure deficit. Plant Cell and Environ **22:** 1515-1526. (1999)

Phillips N, Bond BJ, McDowell NG, Ryan MG. Canopy and hydraulic conductance in young, mature and old Douglas-fir trees. Tree Physiol **22**:205-211 (2002)

Whitehead D, Edwards WRN, Jarvis PG. Conducting sapwood area, foliage area, and permeability in mature trees of *Picea sitchensis* and *Pinus contorta*. Can J For Res **14**:940-947. (1984)

Whitehead D. Regulation of stomatal conductance and transpiration in forest canopies. *Tree Physiol*. **18**:633-644. (1998)

Cowan I. R., Givnish T. J., Economics of carbon fixation in higher plants, in *On the economy of plant form and function* (Cambridge University Press, Cambridge, 1986), pp. 133-170.

West G.B., Brown J.H., Enquist B.J., A general model for the structure and allometry of plant vascular systems. *Nature* **400**, 664-667 (1999).

SI 4: The results shown in Figure 2 are all from the Sevilleta Long Term Ecological Research (LTER) project at the Sevilleta National Wildlife Refuge in central New Mexico, USA (Pangle et al. 2012). Our experimental plots were established on the eastern slope of the Los Pinos Mountains (34°23′11″ N, 106°31′46″ W) in the northeastern corner of the wildlife refuge at a

mean elevation of 1911m. The site is a piñon pine (*Pinus edulis,* Engelm.) and juniper (*Juniperus monosperma* (Engelm.) Sarg.) woodland, with piñon and juniper basal area and canopy coverage that averaged 20.0 m^2 ha^{-1} and 36.7% respectively across the study site. Climate records (20-yr, 1989-2009) from a nearby LTER meteorological station (Cerro Montoso #42; http://sev.lternet.edu/) indicate a mean annual precipitation total of 362.7 mm/yr. The region is strongly influenced by the North American Monsoon, with a large fraction of annual precipitation occurring in July, August, and September. Mean annual temperature (20-yr) at this nearby LTER site was 12.7 ˚C, with a mean July maximum of 31.0 ˚C and a mean December minimum of -3.3 ˚C. In total, our study site consisted of 12 experimental plots located in three replicate blocks that varied in slope %, aspect, and soil depth. A more detailed description and discussion of the vegetative cover and soil properties at this site have been presented elsewhere (see Pangle et al. 2012 and Plaut et al 2012).

The study utilized four different experimental treatments applied in three replicate blocks. The four experimental treatments included 1) un-manipulated, ambient control plots, 2) drought plots, 3) supplemental irrigation plots, and 4) cover-control plots. The three replicated blocks differed in their slope and aspect. One block was located on south facing slopes, one on north facing slopes, and one in a flat area of the landscape. Drought, cover-control, and irrigation infrastructure was installed in 2007, with drought treatments effectively in place by August 2007. The irrigation system was tested in 2007, and supplemental irrigations began in year 2008.

To effectively reduce water availability to trees, we constructed three replicated drought structures that covered an area of 40 m × 40 m (1600 m^2). Each drought plot consisted of 29 parallel troughs running across the 40 m plot, constructed with overlapping 3 ft × 10 ft (0.91 m × 3.05 m) pieces of thermoplastic polymer sheets fixed to horizontal rails that were approximately 1m in height. The plastic sheets were bent into a concave shape to collect and divert the precipitation off plot. The total plastic coverage in each plot is ~45% (± 1%) of the 1600 m^2 plot area, resulting in ~55% of ambient precipitation reaching the ground in drought plots. For an in-depth discussion that compares the severity of our experimentally imposed drought to historical drought conditions observed in the past 100 years, please see Plaut et al. 2013.

In addition, we built cover-control infrastructures to investigate the impact of the plastic drought structures independent of changes in precipitation. The cover-control treatment had the same dimensions as the drought plots, with plastic attached to the rails in a convex orientation so precipitation would fall off the plastic and onto the plot, thus these plots received the same amount of precipitation as un-manipulated ambient plots. Our irrigation system consisted of above-canopy sprinkler nozzles configured to deliver a supplemental rainstorm event of 19 mm (~rate of 19mm hr^{-1}). Our supplemental water was trucked to site and stored in above ground tanks prior to irrigation events. Supplemental irrigations (19 mm $event^{-1}$) were applied through-out the growing season (~ monthly intervals) at an annual rate of 57, 69.5, 112, 107, and 95 mm yr^{-1} from years 2008 thru 2012. At no time did we attempt to alter the timing or the onset of either pre-monsoon or monsoon season precipitation events; our supplemental irrigations were only intended to alleviate plant water stress during the entire frost-free growing season.

Multiple physiological characteristics of ten sample trees (five piñon and five juniper) within each plot were monitored by automated sensors and periodic manual measurements to assess tree responses to precipitation manipulations. Leaf level gas exchange was measured from 2010 through 2012 using standard approaches explained in Limousin et al. (2013). We performed periodic assessments of canopy greenness and canopy dieback (for the same sample

trees) during each growing season (across all plots). Accordingly, across all replicate blocks, a total of n=120 trees (n=60 per species) were initially designated and monitored across the 6+ year duration of the study. For each treatment factor, a subset of n=30 monitored trees (n=15 per species) within this group were subjected to each level of precipitation manipulation (i.e., ambient, drought, supplemental irrigation, and cover-control treatment). And, when available within a given experimental plot, extra replacement trees were designated and monitored in place of original sample trees that experienced either mortality or severe canopy dieback over the 6+ yr duration of the experiment.

Predawn (Ψ_{PD}) and mid-day (Ψ_{MD}) plant water potentials were measured with multiple Scholander-type pressure chambers (PMS Instrument Co, Albany, OR) on excised foliage from sample trees (n=10 per plot) throughout the growing season of each year across all plots. Stem sap-flow (J_S) was measured in sample trees (n=10 per plot) using Granier heat dissipation sap flow sensors installed in 2007 in each plot within the south aspect block (plots 9-12). Trees in north facing (plots 5-8) and flat blocks (plots 1-4) were instrumented with sap-flow sensors during the 2009 season, and the south facing block was re-instrumented with new replacement sapflow sensors in year 2010. All sample trees had two 10 mm Granier sap-flow sensors installed in the outermost sapwood (Granier 1987). Each sensor used the traditional two probe heated and unheated reference design (Granier 1987), with two additional probes located 5 cm to the right side of the primary probes to correct for axial temperature gradients in the stem (Goulden and Field 1994). We found that this compensation for axial temperature gradients is critical to reduce measurement noise resulting from the open-canopy and high radiation environment of this ecosystem. In addition, stems were wrapped with reflective insulation (Reflectix Inc., Markleville, IN) in an effort to shield sap-flow probes from short term ambient temperature fluctuations and direct solar irradiance. Sap-flow (J_S) was calculated according to the methods outlined in Granier (1987) and Goulden and Field (1994). Sapwood depth was greater than 10 mm on the majority of instrumented trees, thus only a very small % of measurements across the 2007-2012 period required a correction due to sensor installation in non-functional stem heartwood (see Clearwater et al. 1999). All data from sap-flow sensors was recorded using Campbell Scientific AM16/32 multiplexers and CR1000 dataloggers (Campbell Scientific, Logan, UT). Data processing was performed using Matlab software (R2011a; The Mathworks, Natick, MA, USA).

Plant hydraulic conductance (K_S, units of mol m^{-2} s^{-1} MPa^{-1}) was calculated using the following relationship based on Darcy's law (Wullschleger et al. 1998, Sperry et al. 2002);

$$K_S = E / (\Psi_{PD} - \Psi_{MD}),$$

with E equal to midday J_S (per unit sapwood area) measured from 1100-1400 hours, and Ψ_{PD} and Ψ_{MD} representing soil (Ψ_S) and midday leaf (Ψ_{MD}) water potential respectively. Due to the short stature of our sample trees (mean height = 4.0 m, range 2.2 to 6.3 m), we did not consider or account for height/gravitational effects in our K_S assessments. For calculations of K_S, only measurements with a midday water potential gradient of least 0.5 MPa difference between Ψ_{PD} and Ψ_{MD} ($\Delta\Psi$) were retained in the analysis. The use of a 0.5 MPa $\Delta\Psi$ gradient threshold served to minimize erroneous K_S estimates that would result from the use of small denominator estimates in calculations (i.e., particularly small $\Delta\Psi$ values). Furthermore, a 0.5 MPa $\Delta\Psi$ cut-off served to remove a significant % of periods where stomata were closed at midday due to drought conditions. Thus these estimates are conservative.

Percentage loss of conductance was estimated as the ensemble product of five model simulations: Sperry, MuSICA, TREES, ED(X), and CLM(ED). These simulations were highly tuned using on-site measurements and represent whole-tree hydraulic conductance loss. More details can be found in (*13*).

Leaf samples for starch analysis were collected approximately monthly from all target trees on ambient, irrigation, and drought plots in block three starting in February 2007. Collections began on all target trees in the other two blocks in 2009. In 2009 and 2010, winter collections were excluded and sampling was focused on seasonal changes during the growing season, with collections in spring (March-April), pre-monsoon (May-June), monsoon (July-Sept), and post-monsoon (Oct-Nov) periods. There was no spring collection in 2010. Cover control samples were collected on the first four sampling dates in 2009. These samples did not reveal significant differences in nonstructural carbohydrate (NSC) from ambient samples, and so sampling was discontinued on cover control plots after June 2009. To reduce the number of samples for analysis, samples from trees on non-drought plots (ambient, cover control, irrigation) and the drought plot in block one (because no trees on the plot had died as of the 2011 growing season) were pooled by plot, species, tissue, and date. This pooling reduced sample number on these plots from 5 to 1 within a given plot, species, tissue and date. The only non-pooled samples were from drought plots in blocks two and three. When trees died (defined as 100% foliar browning; Gaylord et al. 2013) they were excluded from the collection protocol. Piñon sampling was discontinued in August 2009 after the last of the drought trees in blocks two and three had died. Foliar starch was analyzed following the protocol described by Hoch et al. (2002), with minor modifications. All samples were covered in dry ice immediately after collection and stored at -70 °C after transport to the lab. Samples were microwaved at 800 watts for 5 minutes to stop enzymatic activity, then dried at 65 °C for 48 hours and ball-milled to a fine powder (High Throughput Homogenizer, VWR). Samples that were pooled to reduce the number of samples for analysis were thoroughly homogenized after milling. Approximately 12 mg of fine ground leaf material was extracted in a 2mL deep-well plate with 1.6 mL distilled water for 60 minutes in a 100 °C water bath (Isotemp 105, Fisher Scientific). Following extraction, an NAD-linked enzymatic assay was used to evaluate NSC content. NSCs are defined here as free, low molecular weight sugars (glucose, fructose, and sucrose), plus starch. All NSCs were hydrolysed to glucose, linked to the reduction of NAD+ to NADH, and monitored at 340 nm with a spectrophotometer (Cary 50 UV-Vis). Starch was calculated as NSC minus low molecular weight sugars. All NSC content values are expressed as percent of dry matter.

Clearwater, Michael J., Frederick C. Meinzer, José Luis Andrade, Guillermo Goldstein, and N. Michelle Holbrook. Potential errors in measurement of nonuniform sap flow using heat dissipation probes. *Tree Physiology* **19**, no. 10: 681-687. (1999)

Goulden, M. L., and C. B. Field. Three methods for monitoring the gas exchange of individual tree canopies: ventilated-chamber, sap-flow and Penman-Monteith measurements on evergreen oaks. *Functional Ecology*: 125-135. (1994)

Granier, A. Evaluation of transpiration in a Douglas-fir stand by means of sap flow measurements. *Tree Physiology* **3**, no. 4: 309-320. (1987)

Hoch, G., Popp, M. Körner, C. Altitudinal increase of mobile carbon pools in Pinus cembra suggests sink limitation of growth at the Swiss treeline. *Oikos* **98**: 361–374. (2002)

McDowell, Nate G., Rosie A. Fisher, Chonggang Xu, J. C. Domec, Teemu Hölttä, D. Scott Mackay, John S. Sperry et al. Evaluating theories of drought-induced vegetation mortality using a multimodel–experiment framework. *New Phytologist* **200**, no. 2: 304-321. (2013)

Pangle RE, Hill JP, Plaut JA, Yepez EA, Elliot JR, Gehres N, McDowell NG, Pockman WT. Methodology and performance of a rainfall manipulation experiment in piñon-juniper woodland. *Ecosphere* **3**: art28. (2012).

Wullschleger, Stan D., F. C. Meinzer, R. A. Vertessy. A review of whole-plant water use studies in trees. *Tree Physiology* **18**, no. 8-9: 499-512. (1998)

Sperry, J. S., U. G. Hacke, R. Oren, and J. P. Comstock. "Water deficits and hydraulic limits to leaf water supply." *Plant, Cell & Environment* **25**, no. 2: 251-263. (2002)

SI Figure S1: Long-term water potential record and interpretation.

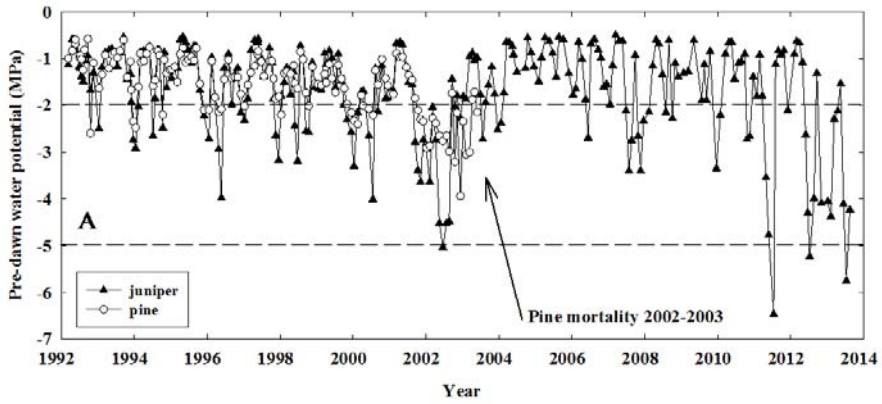

SI Figure S1A) A 21–year time series of monthly pre-dawn Ψ of piñon pine and juniper in Los Alamos, New Mexico, extending prior time series[22,23]. Piñon trees died in 2002-03, with surviving juniper trees becoming the dominants. The species-specific Ψ_{A0} values are presented as horizontal dashed lines. **B)** Dying juniper trees in northern New Mexico in 2013, photo courtesy Mark Watson.

The water potential data shown in SI Figure 1A was collected on a minimum of five trees for pine and another five for juniper (often we sampled around 10 trees each). The methods were identical to those described for the Sevilleta plot (SI 4), except we sample two twigs per tree rather than just one, and average the within tree values. Canopy loss and mortality was observed weekly during the drought events at both sites[21,23]. In pine trees, the entire canopy turns from green to orange within a few weeks, with litterfall happening immediately thereafter.

570 *D* rises exponentially with temperature, thus chronic temperature rise is forcing a particularly
571 rapid rise in D^{20} with implications for Ψ, G_s and survival (equation 1 and Fig. 1B). To ascertain
572 the likelihood of future mortality, we first determined if climate parameters predicted from the
573 Coupled Model Intercomparison Project (CMIP5) multi-model ensembles such as precipitation
574 and *D* could be used to infer our long-term Ψ_{pd} observations (1992-2013). Using the dataset
575 from the long-term monitoring site (SI Fig. 1A) we found annual precipitation and annual mean
576 *D* together explain 70 and 80% of the annual variation in growing-season mean Ψ_{pd} for pine and
577 juniper, respectively (SI Fig. 2). An independent test against the drought manipulation site (Fig.
578 2) also gave a strong predictive relationship for both species (SI Fig. 2). The final relationship
579 using both field sites is:
580
581 pine Ψ_{pd} (april-august) = -10^ [0.993-0.455•log10(ppt)+0.028•*D*] (2),
582 juniper Ψ_{pd} (april-august)=-10^[1.461-0.724•log10(ppt)+0.059•*D*] (3),
583
584 in which annual precipitation (ppt, mm) and *D* (hPa) are total and average, respectively.
585 Equations (2,3) are extremely similar to that used to predict tree ring growth[20], suggesting
586 growth and Ψ_{pd} are coupled and that these variables are broadly applicable.
587

588

589 **SI5:** Regressions for Figure 2.
590 Figure 2B pine: $G_s = 0.345e^{1.66\Psi pd}$, $r^2=0.79$
591 Figure 2B juniper: $G_s = 0.162e^{0.51\Psi pd}$, $r^2=0.80$
592
593 Figure 2C pine: photosynthesis = $2.82*\Psi_{pd}+7.4$, $r^2=0.66$
594 Figure 2C juniper: photosynthesis = $1.287*\Psi_{pd}+7.9$, $r^2=0.74$
595
596 Figure 2D pine: PLC = $-20.23*\Psi_{pd} + 1.80$, $r^2=0.46$
597 Figure 2D juniper: PLC = $-6.42*\Psi_{pd} - 0.20$, $r^2=0.69$
598
599 Figure 2E pine: hydraulic conductance = $0.83e^{0.30\Psi pd}$, $r^2=0.21$
600 Figure 2E juniper: hydraulic conductance = $1.01e^{0.36\Psi pd}$, $r^2=0.36$
601
602 Figure 2F pine: NSC = $1.44*\Psi_{pd} + 6.45$, $r^2=0.14$
603 Figure 2F juniper: NSC = $0.62*\Psi_{pd} + 7.21$, $r^2=0.06$
604

605 **SI6**: Foliar starch has proven a robust indicator of the carbon starvation process in piñon pine
606 (Adams et al. 2013; McDowell et al. 2013; Sevanto et al. 2014; Dickman et al. 2014), and
607 redwood (Quirk et al. 2013) but may underestimate the process in some conifers (e.g. Hartmann
608 et al. 2013).

609 H.D. Adams, *et al*. 2013. Nonstructural leaf carbohydrate dynamics of *Pinus edulis* during
610 drought-induced tree mortality reveal role of carbon metabolism in mortality mechanism. *New*
611 *Phytologist* 197: 1142-1151.

H. Hartmann**,** Trumbore, S. and Ziegler, W. (2013) Lethal drought leads to reduction in nonstructural carbohydrates (NSC) in Norway spruce tree roots but not in the canopy. Functional Ecology 27: 413-427.

L.T. Dickman, N.G. McDowell, S. Sevanto, R.E. Pangle, W.T. Pockman. 2014. Carbohydrate dynamics and mortality in a piñon-juniper woodland under three future precipitation scenarios *Plant, Cell and Environment,* DOI: 10.1111/pce.12441.

N.G. McDowell, Fisher RA, Xu C, Domec JC, Hölttä T, Mackay DS, Sperry JS, Boutz A, Dickman L, Gehres N, Limousin JM, Macalady A, Martinez-Vilálta J, Mencuccini M, Plaut JA, Ogee J, Pangle RE, Rasse DP, Ryan MG, Sevanto S, Waring RH, Williams AP, Yepez EA, Pockman WT. 2013. Evaluating theories of drought-induced vegetation mortality using a multi-model-experiment framework. *New Phytologist* 200(2), 304-321

S. Sevanto, McDowell NG, Dickman LT, Pangle R, Pockman WT. 2013. How do trees die? A test of the hydraulic failure and carbon starvation hypotheses. *Plant, Cell and Environment,* doi: 10.1111/pce.12141

J. Quirk, N.G. McDowell, J.R. Leake, P.J. Hudson, D.J. Beerling. Carbon dioxide starvation, drought, and Cenozoic forest retreat. 2013. *American Journal of Botany,* 100: 582-591.

SI Figure S2: Evaluation of model predictions of predawn water potential

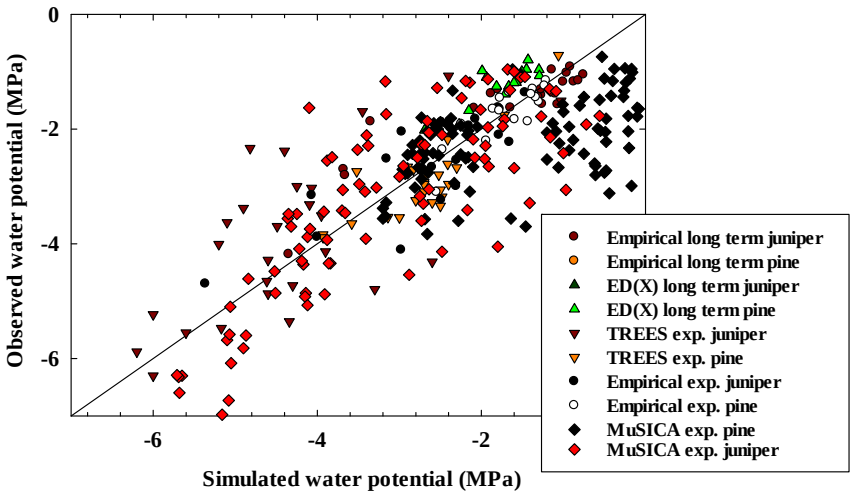

SI Figure 2) Predictions of April through August mean Ψ versus observed Ψ for the long-term (21 year) observations as well as the drought manipulation study for juniper and piñon pine. For pine and juniper, respectively, the empirical water potential approach yielded r^2 values of 0.70 and 0.77, ED(X) simulation yielded r^2 values of 0.82 and 0.77, TREES simulation yielded r^2 values of 0.69 and 0.68, and MuSICA simulation yielded r^2 values of 0.24 and 0.73.

636 Annual growing-season Ψ_{pd} records were developed for each species at the experimental
637 (Sevilleta, SI 4) and long-term observational (Los Alamos, Fig. S1) sites. At the experimental
638 site, a record was developed for each precipitation treatment. Ψ_{pd} measurements were made
639 approximately once per month, generally toward the end of the month. Growing-season records
640 were then calculated by averaging across April–August values. These records covered 1992–
641 2013 at the Los Alamos site and 2007–2013 at the Sevilleta site. For each species, we related the
642 Ψ_{pd} records to seasonal climate data. Based on a priori knowledge of climate responses in the
643 region[20], we developed multivariate equations that estimated growing-season Ψ_{pd} from annual
644 (previous September through growing-season August) precipitation total and mean vapor-
645 pressure deficit (D). We elected to use annual rather than seasonal climate data to avoid over-
646 fitting the multivariate equations. Notably, annually averaged D is dominated by variability in
647 the warm-season, which is when the ecological influence of D variability appears to be strongest
648 in the region[20].

SI 7: Model-specific developments and application

Table S1: A summary of how empirical variables were utilized or simulated by models. The model input parameters are typically static (e.g. soil texture), model driver parameters typically change over time (e.g. micrometeorological data), and model output represents simulated variables. See [13] for more details.

Variable	TREES	MuSICA	ED(X)
Mortality	n/a	n/a	Output
LAI	Input	Input	Output
Density	n/a	Input	Input
Height	Input	Input	Input
Cover	n/a	n/a	Output
NSC	Output	Output	Output
SLA	Input	Input	Input
Ψ_{pd}, Ψ_{md}	In/Output[1]	Output	Output
E[2]	In/Output[1]	Output	Output
Respiration	Output	In/Output	n/a
Vcmax	Input	Input	Input
Vulnerability	Input	Input	Input
Ψ_{soil}	Output	Output	Output
SWC	Output	Output	n/a
Soil depth	Input	Input	Input
Soil temp.	Input	Output	n/a
Soil texture	Input	Input	Input
Allometry	Input	Input	Input
Air temp.	Driver	Driver	Input
VPD	Driver	Driver	Input
PAR	Driver	Driver	Input
Wind speed	Driver	Driver	Input
Atm Press.	Driver	Driver	Input
Hyd Cond	Output	Output	Input

[1] Ψ_{pd}, Ψ_{md}, and E at saturated hydraulic conductance (K) input; values at other times output
[2] Used for evaluation of all models

Model specific developments and application

TREES: The Terrestrial Regional Ecosystem Exchange Simulator (TREES) (Samanta *et al*., 2007; Loranty *et al*., 2010; Mackay *et al*., 2012; Roberts 2012) is a dynamic model of plant water and carbon flows. A unique methodological improvement in TREES is a full coupling of the Sperry *et al*. (1998) model of plant water balance and cavitation with stomatal conductance (G_S), photosynthesis (A), and E driven by energy supply and vapor demand. Thus, TREES explicitly incorporates A and dynamic plant hydraulic conductance into a unified numerical solution. It also predicts *PLC*, *NSC*, growth efficiency, and carbon allocation to leaves, roots, and stem. The model was calibrated using pre-drought gas exchange, transpiration, water potentials,

and vulnerability curve measurements (Plaut *et al*., 2012, Limousin *et al*., 2013). Root-to-leaf area (RL) ratios for each species were optimized to maximize carbon uptake for a given amount of water loss, a conservative approach that is appropriate for the dry Southwest climates. This analysis predicted an optimal root RL of 2 for pine and 3 for juniper. TREES was set up to re-adjust the plant hydraulic conductance once per year, in early spring (on year-day 60), to account for refilling. The rooting zone had a maximum depth in the shallow simulations of 19cm, and a maximum depth in the deep simulations of 89cm. Soil water balance was updated in each half-hour time step for each layer using precipitation inputs, drainage, and rhizosphere fluxes. Water potentials, hydraulic conductances, and fluxes were calculated based on the updated soil moisture, cavitation status, and transpiration demand. Allocation of carbon to leaves was allowed to adjust upward based on available NSC and downward with increasing PLC. Root area was recomputed annually using the updated leaf area and the pre-set optimal RL.

MuSICA: The MuSICA model is a multilayer, multi-leaf process-based biosphere-atmosphere gas exchange model that simulates the exchanges of mass (water, CO_2) and energy in the soil-vegetation-atmosphere continuum (Ogée *et al*., 2003). The version of the model used in this study includes a more detailed description of root water uptake and plant water storage dynamics, as well as soil water hydraulic redistribution and root cavitation (Domec *et al*., 2012; McDowell et al. 2013) and plant *NSC* storage dynamics (Ogée *et al*., 2009; McDowell et al. 2013). Stand density, biomass, leaf area, and soil properties were taken from Pangle *et al*. (2012) and Plaut *et al*. (2012). The model was calibrated using pre-drought gas exchange and photosynthetic parameters, stomatal response to water potentials and vulnerability curve measurements (Plaut *et al*., 2012, Limousin *et al*., 2013). Maximum rooting depth and root distribution for both species were taken from Plaut et al. (2012). Both species were modeled at the same time and thus competed for the same soil water.

To evaluate the model performance we forced the MuSICA model with meteorological values (radiation, wind speed, temperature, humidity, precipitation) collected at the site and quantified its ability to reproduce midday and predawn leaf water potentials and daily tree transpiration measured on each species between 2007 and 2011 (e.g., see SOM Fig. 2).

For the simulations shown in the main text, we forced MuSICA with two CMIP5 climate scenarios (see main text) assuming either shallow or deep rooting depths for both species, and all other parameters being equal. Mortality rates for each species were computed as with the other models, using predawn leaf water potential predictions from MuSICA over the four simulations (2 climate scenarios × 2 rooting depths).

ED(X): The Ecosystem Demography (ED) model tracks cohorts of trees based on their sizes (Moorcroft *et al*., 2001). ED(X) simulates tree mortality of cohorts based on the assumption of carbon starvation (Fisher *et al*., 2010) and hydraulic failure (Xu *et al.* 2013). To better present the seasonal cycles of carbon storage, instead of using *GPP* directly for growth, it is first all fed into the *NSC* pool, which is then used by respiration and growth of new tissue determined by carbon sink strength (*13*). Plant hydraulics and hydraulic failure are simulated using existing theories on plant water storage (Meinzer *et al.* 2003) and hydraulic conductivity (Sperry *et al.* 1998). Specifically, the model simulates water storage in tree xylem, which declines during drought due to leaf and root water loss. The reduced water content can lead to cavitation (forming of bubbles in xylem conduits), which impairs the xylem conductivity (Sperry 2000). If

the amount of cavitation passes a critical threshold, xylem becomes dysfunctional and hydraulic failure ensues (Urli *et al.* 2013). The model is first tuned to fit the Sevilleta data of predawn leaf water potential. Then it is applied for the independent long-term observation site at Los Alamos shown in SI Fig. 1A for model evaluation, with different soil depth and texture.

Domec J-C, Ogée J, Noormets A, Jouangy J, Gavazzi M, Treasure E, Sun G, McNulty S, King JS. Interactive effects of nocturnal transpiration and climate change on the root hydraulic redistribution and carbon and water budgets of Southern US pine plantations. *Tree Physiology* **32**: 707-723. (2012)

Fisher R, McDowell N, Purves D, Moorcroft P, Sitch S, Cox P, Huntingford C, Meir P, Woodward FI. Assessing uncertainties in a second-generation dynamic vegetation model caused by ecological scale limitations. *New Phytologist* **187**: 666-681. (2010)

Limousin JM, Bickford CP, Dickman LT, Pangle RE, Hudson PJ, Boutz AL, Gehres N, Osuna JL, Pockman WT, McDowell NG. Regulation and acclimation of leaf gas-exchange in a piñon-juniper woodland exposed to three different precipitation regimes. *Plant, Cell & Environment,* DOI: 10.1111/pce.12089. (2013)

Loranty MM, Mackay DS, Ewers BE, Traver E, Kruger EL. Competition for light between individual trees lowers reference canopy stomatal conductance: results from a model. *Journal of Geophysical Research - Biogeosciences* **115**: G04019, doi:10.1029/2010JG001377 (2010).

Mackay DS, Ewers BE, Loranty MM, Kruger EL, Samanta S. Bayesian analysis of canopy transpiration models: A test of posterior parameter means against measurements. *Journal of Hydrology* **432-433**: 75-83 (2012)

McDowell, Nate G., Rosie A. Fisher, Chonggang Xu, J. C. Domec, Teemu Hölttä, D. Scott Mackay, John S. Sperry et al. Evaluating theories of drought-induced vegetation mortality using a multimodel–experiment framework. *New Phytologist* 200, no. **2**: 304-321. (2013)

Meinzer, F. C.; James, S. A.; Goldstein, G.; Woodruff, D., Whole-tree water transport scales with sapwood capacitance in tropical forest canopy trees. *Plant Cell Environ*, **26**(7), 1147-1155. (2003)

Moorcroft PR, Hurtt GC, Pacala SW. A method for scaling vegetation dynamics: the ecosystem demography model (ED). *Ecological Monographs* **71**: 557-585. (2001)

Ogée J, Brunet Y, Loustau D, Berbigier P, Delzon S. MuSICA, a CO_2, water and energy multi-layer, multi-leaf pine forest model: evaluation from hourly to yearly time scales and sensitivity analysis. *Global Change Biology* **9**: 697–717. (2003)

Ogée J, Barbour MM, Wingate L, Bert D, Bosc A, Stievenard M, Lambrot C, Pierre M, Bariac T, Loustau D *et al*. A single-substrate model to interpret intra-annual stable isotope signals in tree-ring cellulose. *Plant, Cell & Environment* **32**: 1071-1090. (2009)

Pangle RE, Hill JP, Plaut JA, Yepez EA, Elliot JR, Gehres N, McDowell NG, Pockman WT. Methodology and performance of a rainfall manipulation experiment in piñon-juniper woodland. *Ecosphere* **3**: art28. (2012)

Plaut JA, Yepez EA, Hill J, Pangle R, Sperry JS, Pockman WT, McDowell NG. Hydraulic limits preceding mortality in a piñon-juniper woodland under experimental drought. *Plant, Cell and Environment* **35**: 1601-1617. (2012)

Roberts. *Development of a coupled ecosystem exchange plant hydraulic model to explore drought related plant mortality*. Master Thesis, University at Buffalo, Buffalo, NY, USA. (2012)

Samanta S., Mackay DS, Clayton M, Kruger EL, Ewers BE. Bayesian analysis for uncertainty estimation of a canopy transpiration model. *Water Resources Research* **43**: W04424, doi:10.1029/2006WR005028. (2007)

Sperry JS, Adler FR, Campbell GS, Comstock JP. Limitation of plant water use by rhizosphere and xylem conductance: results from a model. *Plant Cell & Environment* **21**: 347-359. (1998)

Sperry, J. S., Hydraulic constraints on plant gas exchange. *Agric For Meteorol,* **104**, (1), 13-23. (2000)

Urli, M.; Porté, A. J.; Cochard, H.; Guengant, Y.; Burlett, R.; Delzon, S., Xylem embolism threshold for catastrophic hydraulic failure in angiosperm trees. *Tree Physiol, 10.1093/treephys/tpt030*. (2013)

Xu, Chonggang, Nate G. McDowell, Sanna Sevanto, and Rosie A. Fisher. Our limited ability to predict vegetation dynamics under water stress. *New Phytologist* **200**, no. 2: 298-300. (2013)

Detailed model descriptions:

TREES: The Terrestrial Regional Ecosystem Exchange Simulator (TREES) (Mackay *et al*., 2003; Samanta *et al*., 2007; Loranty *et al*., 2010; Mackay *et al*., 2012) that operates as a physiology model at the scale of individual trees or as an ecosystem model for whole stands. At the plant scale the model couples photosynthesis, stomatal conductance, and transpiration in a steady state solution for sun and shade canopy at 30-minute time steps, and forced with micrometeorological data (air temperature, wind speed, radiation, vapor pressure deficit, and soil temperature). This coupled canopy model and the plant water balance model (Sperry *et al*., 1998) were combined into a single, integrated model to explicitly simulate soil-plant hydraulics and hydraulic failure, and to provide both demand and supply limits on stomatal control of carbon uptake and water loss (Roberts, 2012), as well as carbon utilization and allocation.

At the whole plant canopy scale stomatal conductance (G_S) was calculated by combining Darcy's Law and Fick's law of diffusion as

$$G_S = K_L (\Psi_S - \Psi_L)/D \quad (1)$$

where $K_L(\Psi)$ and Ψ_L are whole-plant hydraulic conductivity and leaf water potential, respectively; D is vapor pressure deficit in the canopy; and Ψ_S is soil water potential integrated over the rooting depth of the plant. The canopy and plant water balance model components are solved iteratively until they converge on a transpiration rate, with simultaneous solution of photosynthesis and stomatal conductance. For this study TREES discretized each modeled tree into three root modules, each having an absorbing and conducting element, and one canopy module having a conducting element and a lateral element with sun and shade sub-elements for gas exchange. The rhizosphere around each absorbing root element was discretized into five sub-

elements for transporting water between the bulk soil and the absorbing root (see Sperry *et al.*, 1998 for details). The root zone soil water balance was maintained by the model and updated, in separate layers defined by discrete root depth, using rhizosphere flux rates determined as part of the plant water balance model solution. The model moves water at the soil-root interface either from soil to root or from root to soil as a function of the pressure gradients. Once the plant hydraulic solution converges the photosynthetic assimilation is accumulated and for daily updating of NSC.

Plant mortality due to hydraulic failure can be predicted using TREES because of cavitation. Plant mortality due to carbon starvation is not explicitly modeled. However, changes in NSC are simulated as the difference in carbon uptake and utilization. A reduction in carbon uptake occurs when stomatal closure reduces photosynthetic assimilation of carbon. Using hydraulic conductance as a proxy for carbon transport reduces carbon utilization. Consequently, as a simulated tree approaches a condition that suggests that it would be susceptible to mortality due to stomatal closure and reduced water for carbon transport, both carbon uptake and utilization decline, which means the rate of change of NSC can be negligible. Although this would not directly predict mortality due to carbon starvation a combination of plant hydraulic conductivity, hydraulic safety, cavitation, changes in NSC, carbon uptake, and carbon use collectively can be used to diagnose the health status of a simulated tree.

Changes in NSC for the whole plant were calculated at daily time steps as

$$dC_{NS}/dt = C_A - C_G - C_M \quad (2)$$

where C_{NS} is NSC, C_A is photosynthetically assimilated carbon for period t (*i.e.* 1 day), C_G is growth and growth respiration allocated in time t, and C_M is maintenance respiration over period t. Carbon is allocated first to C_M and then to C_G. C_M was calculated using separate temperate-based respiration rates for leaf, stem, and roots as

$$C_M = (R_{root}\, C_{root}\, r^{Troot} + R_{stem}\, C_{stem}\, r^{Tstem}\, e^{0.67*\log(10C_{stem})}/10 + R_{leaf}\, C_{leaf}\, r^{Tleaf})\, f_{M\sim K} \quad (3)$$

where R terms refer to root, stem, and leaf intrinsic respiration rates (fraction), C terms are carbon pools, T terms are temperatures, r is a respiration coefficient, and $f_{M\sim K}$ is a function that reduces the transport of NSC to sites for maintenance respiration as a function of hydraulic conductivity and saturated hydraulic conductivity K_{Lsat} as

$$F_{M\sim K} = K_L(\Psi)/K_{Lsat} \quad (4)$$

When root temperature is at least 5 ºC, then C_G is calculated as a parameterized fraction (β_G) of C_A as

$$C_G = \beta_G C_A f_{G\sim K} \quad (5)$$

where $f_{G\sim K}$ is function that reduces the transport of NSC to sites for growth as a function of hydraulic conductivity and saturated hydraulic conductivity K_{Lsat} as

$$f_{G\sim K} = [K_L(\Psi)/K_{Lsat}]^2 \quad (6)$$

TREES was parameterized and run on individual trees using individual tree data to the extent possible. The model was tuned to each tree using species-specific allometric equations and the basal area of each respective tree, and sap flux data for each respective tree. TREES carbon pools were initialized for each individual tree using allometric equations for the root, stem, and leaf structural carbon pools and measured NSC (McDowell *et al.***,** ***unpublished data***). TREES was parameterized for hydraulics by species using vulnerability to cavitation curves (Plaut *et al*., 2012), and by individual tree using sap flux data to obtain midday transpiration at saturated hydraulic conductivity. Measured pre-dawn and mid-day water potentials at saturated hydraulic conductivity were also used. Site-specific soil texture data was used to parameterize the soil hydraulic properties. The photosynthesis routines were parameterized using species and treatment specific data collected in the study. All canopy calculations were expressed on a per unit leaf area basis, and so leaf area index by individual tree was obtained from allometry and taking the calculated total leaf area divided by projected crown area (Loranty *et al*., 2010; Mackay *et al*., 2010). We assumed that each tree operated independently of its neighbors, and so there were no interactions between root uptake rate among trees. The trajectory of carbon and water pools and fluxes for each tree was therefore independently calculated, and determined as a function of each respective tree's carbon pools, hydraulic properties, and effect on its local soil water conditions.

MUSICA: The multilayer, multi-leaf, process-based biosphere-atmosphere gas exchange model MuSICA has been primarily developed to simulate the exchanges of mass (water, CO_2) and energy in the soil-vegetation-atmosphere continuum and is particularly well designed for studies on conifer trees because it deals with needle clumping of various needles cohorts (Ogée *et al*., 2003). MuSICA assumes the terrain to be relatively flat and the vegetation horizontally homogeneous. Several species can share a common soil and the mixed canopy is partitioned into several vegetation layers (typically 10-15) where several leaf types (sunlit/shaded, wet/dry) for each cohort and species are distinguished. Stand structure is therefore explicitly accounted for and competition for light and water between species can be explored. The version of MuSICA used in this study is the same as in other studies (e.g. Domec *et al*., 2012; McDowell et al. 2013). It typically produces output at a 30-min time step and can be run over multiple years or decades as long as the vegetation structure is given. A brief overview of the different sub-models embedded in this MuSICA version is given below.

The radiative transfer scheme is based on the radiosity method and supports multiple (broad-leaf or needle-leaf) species in a given vegetation layer (Sinoquet *et al*., 2001). Rain interception and canopy evaporation are computed for each species and vegetation layer using the concept of maximum storage capacity (Rutter et al. 1971). Vertical profiles of the microclimate (air temperature, humidity and CO_2) within the vegetation canopy are computed using the Lagrangian near-field theory (Raupach 1988). A multilayer, coupled heat and water soil transport model that explicitly accounts for root water uptake for each species is also implemented. Water storage in the plants is accounted for using a single water storage capacity for each species that scales with leaf area (Williams *et al*., 2001). The soil water retention curve and the unsaturated soil hydraulic conductivity are described according to the model of Van Genutchen (1980). The leaf-to-air energy, water and CO_2 exchange model consists of a photosynthesis model (Farquhar *et al*., 1980), a stomatal conductance model (Leuning, 1995), a leaf boundary-layer model (Nikolov *et al*., 1995) and a leaf energy budget equation. Species-specific photosynthetic parameters are the maximum rates of carboxylation and electron transport, mitochondrial respiration and quantum yield. All these parameters vary with leaf temperature and/or leaf ontogeny and are thus prescribed at a given temperature (25°C) and for young and old leaves or needles. Day respiration is computed using the night respiration rate parameterization and a light inhibition factor. Woody respiration is scaled using living biomass, basal respiration rates and Q_{10} values and is assumed to depend on air temperature only. Soil and litter respiration rates are a function of soil temperature and soil moisture. Soil water deficit affects the maximum stomatal conductance and photosynthetic capacity and is described by a sigmoid curve of leaf water potential, with a common threshold and slope for both variables. Soil water deficit also induces root cavitation that is described by Weibull-like curves of plant water potential (Domec & Gartner 2001).

The parameterisation of the model was done as follows. Stand density, woody biomass, leaf area, and soil properties were taken from Pangle *et al*. (2012) and Plaut *et al*. (2012). Maximum rooting depth and root-to-shoot area ratios were taken from Plaut et al. (2012). Living tissue respiration was parameterized using basal respiration rates determined at the site (McDowell et al. 2013). Soil and litter respiration rates were parameterized from soil respiration data collected at the site in 2006 and 2007 (White, 2008). Stomatal conductance and photosynthetic parameters (maximum rates of carboxylation, rate of photosynthetic electron transport and mesophyll conductance) were taken from Limousin et al (2013).

To evaluate the model performance we forced the MuSICA model with meteorological values (radiation, wind speed, temperature, humidity, precipitation) collected at the site and quantified its ability to reproduce midday and predawn leaf water potentials and daily tree transpiration measured on each species between 2007 and 2011 (e.g., see SOM Fig. 2).

For the simulations shown in the main text, we forced MuSICA with two CMIP5 climate scenarios (see main text) assuming either shallow or deep rooting depths for both species, and all other parameters being equal. Mortality rates for each species were computed as with the other models, using predawn leaf water potential predictions from MuSICA over the four simulations (2 climate scenarios × 2 rooting depths).

Dewar RC, Medlyn BE, McMurtrie RE. A mechanistic analysis of light and carbon use efficiencies. Plant, Cell and Environment , **21**: 573–588 (1998).

Domec JC, Gartner BL (2001) Cavitation and water storage capacity in bole xylem segments of mature and young Douglas-fir trees. *Trees*, **15**: 204–214 (2001).

Farquhar, G.D., S. von Caemmerer and J.A. Berry. A biochemical model of photosynthetic CO2 assimilation in leaves of C3 species. Planta **149**, 78–90 (1980).

Leuning, R. A critical appraisal of a combined stomatal-photosynthesis model for C3 plants. Plant Cell Environ. **18**:339–356 (1995).

McDowell, Nate G., Rosie A. Fisher, Chonggang Xu, J. C. Domec, Teemu Hölttä, D. Scott Mackay, John S. Sperry et al. Evaluating theories of drought-induced vegetation mortality using a multimodel–experiment framework. *New Phytologist* 200, no. **2**: 304-321 (2013).

Sinoquet H, Le Roux X, Adam B, Ameglio T, Daudet F. RATP: a model for simulating the spatial distribution of radiation absorption, transpiration and photosynthesis within canopies: application to an isolated tree crown. *Plant Cell Environ*., **24**: 395–406 (2001).

Williams, M., E.B. Rastetter, G.R. Shaver, J.E. Hobbie, E. Carpino B.L. Kwiatkowski. Primary production in an arctic watershed; an uncertainty analysis. Ecol. Appli. **11**: 1800-1816 (2001).

Wingate, L., Oǵee, J., Burlett, R., Bosc, A., Devaux, M., Grace, J., Loustau, D., and Gessler, A. Photosynthetic carbon isotope discrimination and its relationship to the carbon isotope signals of stem, soil and ecosystem respiration, New Phytol., **188**, 576–589 (2010).

ED(X): ED(X) generated the most conservative forecasts, with the likelihood of pine mortality approaching 100% (for the average grid cell) by 2078 and only 31% likelihood of juniper mortality by 2100. We used the Ecosystem Demography (ED) model (Moorcroft *et al*., 2001) with modifications described by Fisher *et al*. (2010), McDowell et al (2013) and Xu et al (2013). The model simulates a water storage pool for the plants and calculates the xylem water potential changes based on the relative water content in xylem (Barnard et al 2011). For each 30-minutes time step, the model simulates leaf water potential based on the water balance, which is calculated as the difference between water supply as determined by the Ball-Berry stomata conductance and vapor pressure gradient from leaf to air, and the water demand as determined by the xylem conductance, tree height and the difference between leaf water potential and xylem water potential. The water storage pool is recharged by the root water uptake as determined by the pressure gradient from soil to xylem and the xylem conductance. During the drought, the plant halts photosynthesis if the xylem water potential is lower than minimum leaf water potential with no water recharge from the soil and the water storage will decline due to the loss of water by cuticular transpiration and the root water loss to soil. Regeneration processes were turned off in our simulations because we were focused on the mortality patterns. ED(X) generated the most conservative forecasts in Figure (3), with the likelihood of pine mortality approaching 100% (for the average grid cell) by 2078 and only 31% likelihood of juniper mortality by 2100.

This ED version uses a single soil layer. The soil water potential (ψ_s) is simulated based on an empirical equation as follows (Niu and Yang 2006):

$\psi_s = \psi_{s0}\theta^{-\lambda}$ where ψ_{s0} is the reference soil water potential for saturated soil, θ is the volumetric saturation of water in soil pores, and λ is the exponent determined by soil texture, as follows:

$$\lambda = 2.91 + 0.159\mathrm{P}_{\mathrm{clay}},$$

where $\mathrm{P}_{\mathrm{clay}}$ is the percent of clay in the soil.

The maximum plant water supply is calculated based on the water potential gradient between leaf and xylem and xylem resistance as follows:

$$W_{\mathrm{supp}} = \frac{\psi_x - \psi_{l\min}}{r_c R_x / A_s + R_l}$$

where the denominator represents the water transport resistance from trunk to leaf assuming the transport distance is the tree crown radius. Specifically, R_x is the resistance of water transport in xylem ($m^3 \cdot Mpa \cdot s/ kg$) with A_s representing the sap wood area (m^2). R_l is the resistance of water transport from branch to leaf ($m^3 \cdot Mpa \cdot s/ kg$) and r_c is the crown radius (m).

The xylem conductivity ($\frac{1}{R_x}$) may reduce due to xylem cavitation (Sperry *et al.*, 1998). The proportion loss of conductivity (PLC) is calculated based on the xylem water potential using the Weibull equation as follows (Neufeld *et al.*, 1992):

$$PLC = 1.0 - e^{-(\psi_x/\Phi_{73})^c},$$

where Φ_{73} is the critical soil water potential that cause 73% loss of xylem conductivity and c is the shape parameter for conductivity loss.

The water demand of each leaf layer for a cohort is calculated based on the stomata conductance and relative humidity. Specifically,

$$W_{dem} = \frac{18.0}{r_b + r_s}\frac{(e_s - e_a)}{RT},$$

where r_b and r_s are the boundary layer and stomata resistance of water (*s/m*). R is the gas constant (8, 314 *J/K/kmole*) and *T* is the air temperature (*K*). e_s and e_a are the vapor pressure inside leaf and of the canopy air (*Pa*). r_s is calculated based on the empirical Ball-Berry model (Ball *et al.*, 1987). Specifically,

$$r_s = \frac{1}{C_f}\left(m\frac{A}{C_a}\frac{e_a}{e_s}P_{atm} + 2000\right),$$

where C_a is the CO_2 partial pressure in the canopy air and P_{atm} is the atmospheric pressure (Pa). C_f is the conversion factor from *s/m* to *s·m2 / umol*,

$$C_f = \frac{P_{atm}}{RT}10^9.$$

The xylem water potential is calculated based on the relative water content as follows (Barnard et al 2011):

$$\psi_x = \frac{a(1-RWC)}{1+b(1-RWC)},$$

where RWC is the relative xylem water content.

The xylem water content changes resulting from the balance of xylem water recharge and water loss from root and leaf. The xylem water recharge rate (kg water/s) is calculated based on the water pressure gradient from soil to xylem and the xylem resistance (R_x, m^3·Mpa·s/ kg water) and the soil-root resistance (R_{rs}, *s·MPa/m*),

$$W_{recharge} = \frac{\psi_s - \psi_x + 9.8h/1000}{hR_x/A_s + R_{rs}},$$

where ψ_s is the soil water potential (*MPa*) and *h* is the height of tree (m). If the soil water potential is less than xylem water potential during drought, the xylem water reduces with root and leaf water loss. The root water loss (*kg water/s*) is calculated based on the water potential gradient from root to soil as follows:

$$W_{rloss} = g_r \max(\psi_x - \psi_s, \psi_{sr\_\max}),$$

where g_r is the root water loss rate (*m/s/Mpa*) and the $\psi_{sr\_\max}$ is the maximum water potential gradient between soil and root due to potential isolation of root from soil under very dry conditions (Tardieu and Simonneau 1997). When the xylem water potential become less than prescribed minimum leaf water potential, the stomata closes and r_s is equal to the culticular resistance (r_{s0}). The leaf water loss (W_{lloss}) is calculated based on cuticular resistance (r_{s0}; s/m) and the vapor pressure difference between leaf and air,

$$W_{lloss} = \frac{18.0}{r_b + r_{s0}} \frac{(e_s - e_a)}{RT}.$$

Table S2: Key hydraulic parameter values used for the ED model. See McDowell *et al.* (2013) for parameters of carbon dynamics and allometry.

Parameter	Description	Value for pine	Value for juniper	Sources
$\psi_{l\min}$	Minimum leaf water potential	-2.1	-4.1	Empirical
ϕ_{s0}	critical soil water potential that cause 50% loss of conductivity	-3.57	-8.45	Data
ϕ_s	shape parameter for conductivity loss	4.07	2.2	Data
A	Coefficient for xylem water potential calculation	-0.683	-1.283	(Barnard et al 2011)*
B	Coefficient for xylem water potential calculation	-0.981	-0.981	(Barnard et al 2011)+
r_{s0}	cuticular resistance (s/m)	1.0e6	1.0e6	Data
g_r	Root water loss rate (m/s/Mpa)	1.5e-10	2.5e-10	Fitted to predawn
$\psi_{sr\_\max}$	Maximum water potential gradient between soil and root (MPa)	2	3	Empirical

J. T. Ball, I. E. Woodrow, J. A. Berry, in *Progress in Photosynthesis Research,* J. Biggins, Ed. (Martinus Nijhoff Publishers, Netherlands), vol. 4, pp. 221–224. (1987)

D. M. Barnard *et al.*, Climate-related trends in sapwood biophysical properties in two conifers: avoidance of hydraulic dysfunction through coordinated adjustments in xylem efficiency, safety and capacitance. *Plant Cell Environ* **34**, 643 (2011).

H. S. Neufeld *et al.*, Genotypic variability in vulnerability of leaf xylem to cavitation in water-stressed and well-irrigated sugarcane. *Plant Physiol* **100**, 1020 (1992).

G.-Y. Niu, Z.-L. Yang, Effects of Frozen Soil on Snowmelt Runoff and Soil Water Storage at a Continental Scale. *J Hydrometeorol* **7**, 937 (2006).

J. S. Sperry, F. R. Adler, G. S. Campbell, J. P. Comstock, Limitation of plant water use by rhizosphere and xylem conductance: results from a model. *Plant Cell Environ* **21**, 347 (1998).

F. Tardieu, T. Simonneau, Variability among species of stomatal control under fluctuating soil water status and evaporative demand: modelling isohydric and anisohydric behaviours. *J Exp Bot* **49**, 419 (Mar, 1998).

C. Xu, N. G. McDowell, S. Sevanto, R. A. Fisher, Our limited ability to predict vegetation dynamics under water stress. *New Phytol* **200**, 298 (2013).

SI Figure S3. Examples of simulations used to calculate mortality probability.

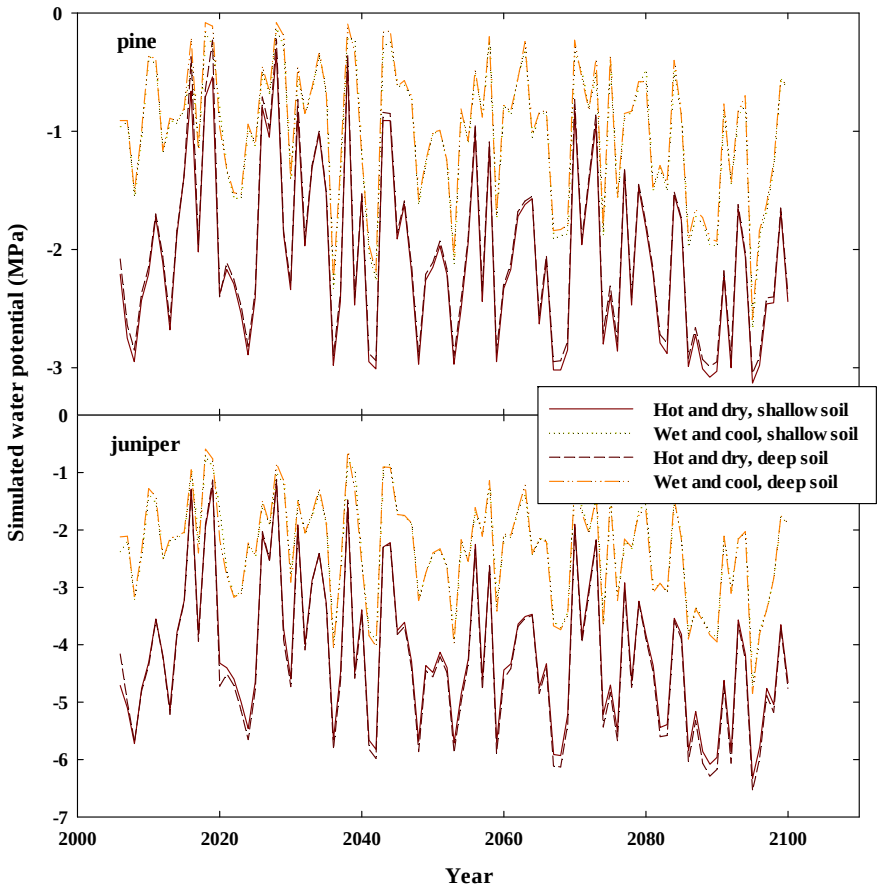

SI Figure S3. An example of the range of simulations of pre-dawn water potential (averaged for April-August) employed to calculate mortality probabilities shown in Figure 3C. In this case, MuSICA was driven with climate data from a wet and cool grid cell and a hot and dry grid cell from Figure (3D), with an assumed soil depth of either 50cm (shallow) or 150cm (deep). Climate is more important than soil depth on simulated Ψ. TREES was driven similarly. ED(X) used climate forecasts for each grid cell shown in Figure (3D) with an assumed soil depth of 50cm.

1055 **SI Figure S4.** Future water potential simulations (April-August average) by each model.

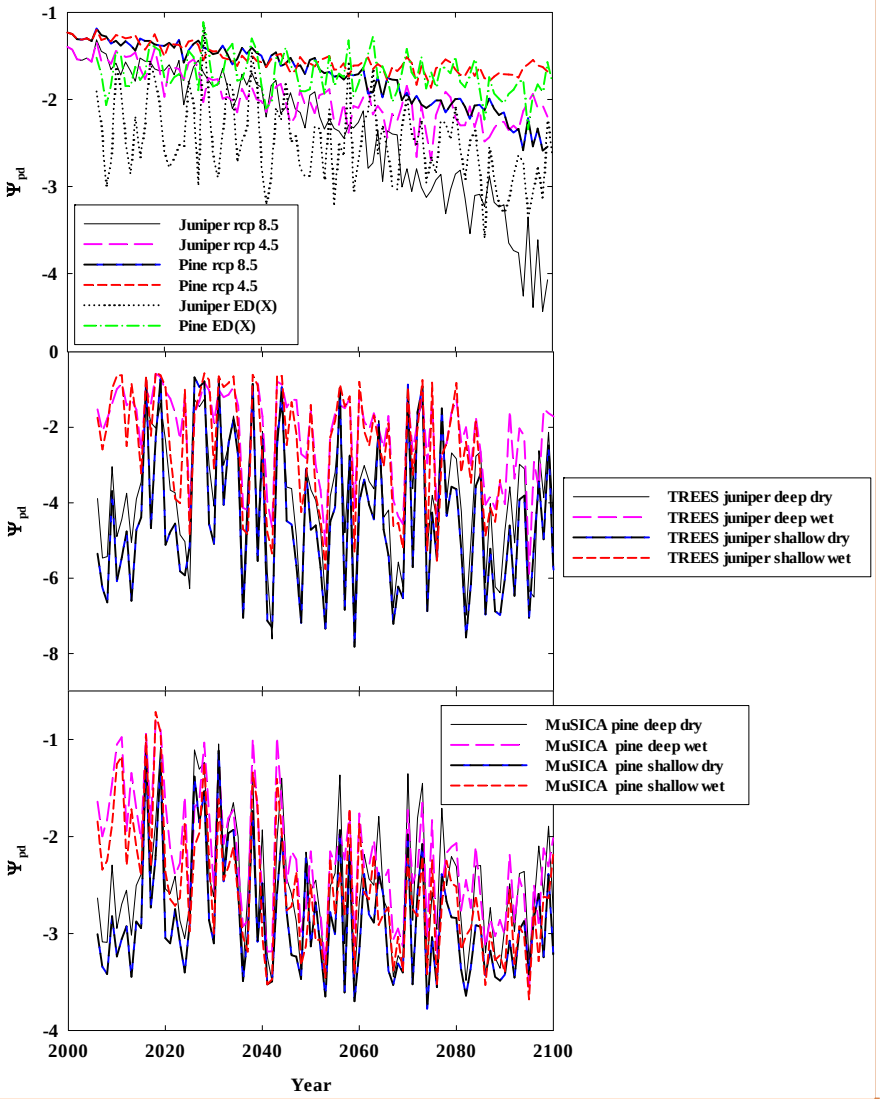

1056

1057 **SI Figure S4 A)** Simulations by the tree-ring based model for both species and for RCP 4.5 and
1058 8.5, as well as by ED(X), **B)** simulations by TREES, **C)** simulations by MuSICA.
1059

Comment [MNG1]: Remember Scott Mackay was concerned with one of these figures, try to fix it.

SI Figure S5. Survival likelihood is sensitive to origination year (2006 vs 2014).

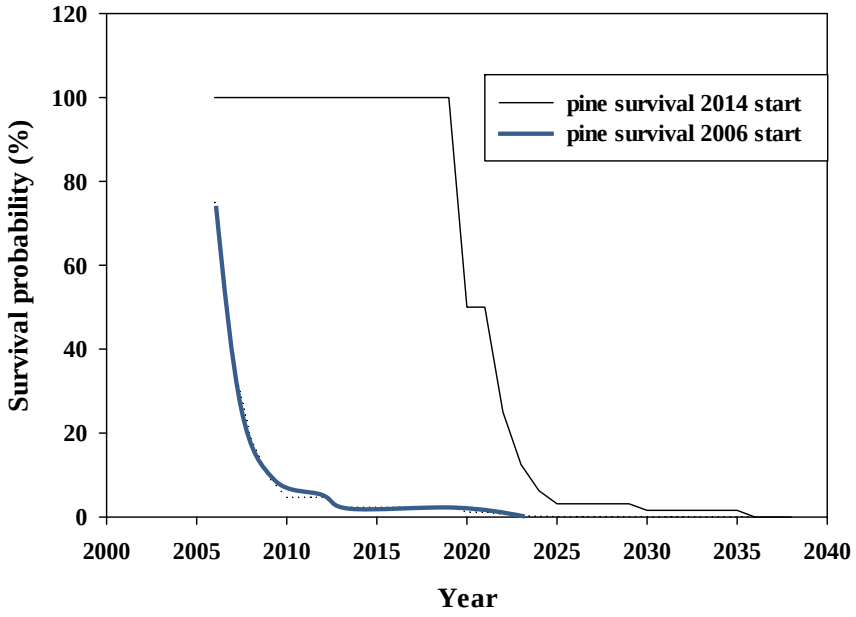

SI Figure S5. Survival probability was calculated either starting in 2006 or 2014, during the interim CMIP5 predicted multiple years of drought. Simulations are shown using the empirical model; however, all models showed the same sensitivity to the origination year of the calculations of mortality. This indicates the results presented in Figure 3C are very conservative because all model calculations of mortality probability used 2014 as a start date rather than 2006.

SI 8: In all cases future predictions of mortality relied on CMIP5 predictions of future climate. The empirical calculation used all 16 model predictions of future climate, predicted mortality probability, and then averaged them. TREES and MuSICA used a particularly hot and dry, and a particularly wet and cool, grid cell, respectively, from the CMIP5 predictions for the piñon-pine-juniper woodlands. They then assumed either 50 cm or 150 cm soil depths, respectively. The odds of Ψ crossing the species-specific thresholds were then summed across the permutations for each time step (year) and combined multiplicatively over time. ED(X) did a similar exercise but for 71 different grid cells in the piñon-pine-juniper woodland region. The empirical calculation used the CMIP5 predictions for the entire piñon-pine-juniper woodland region and equations (SI 2,3).

SI Figure S6. Comparison of mortality probability predicted by the empirical method using RCP8.5 (business as usual) vs. RCP4.5 (moderate emissions controls).

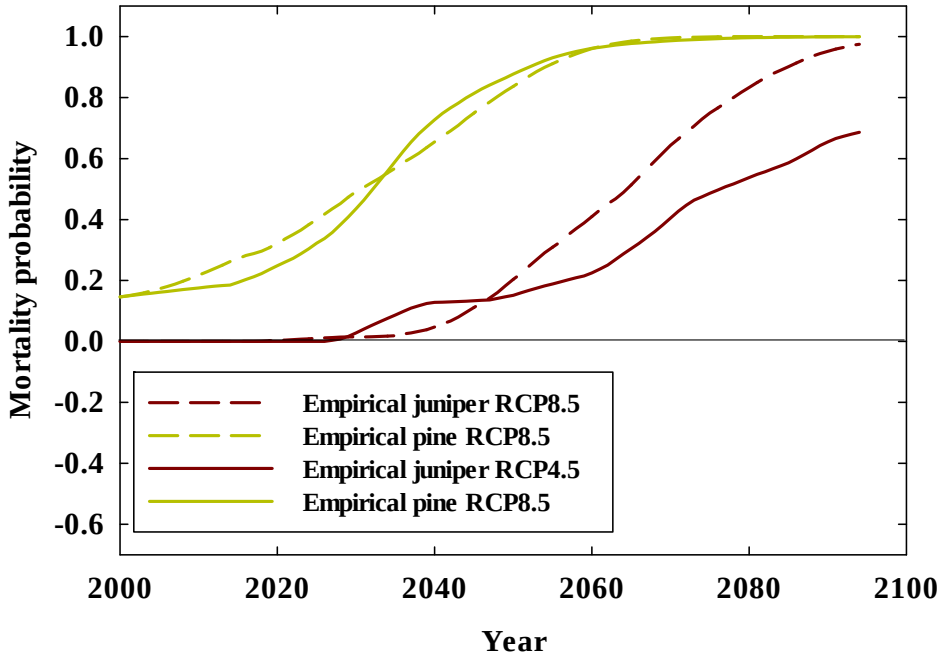

SI Figure 7. ED(X) simulations shown in Figure 3D are replicated here with the same color coding for number of mortality events between 2066-2095, except plotted here is the mean temperature and precipitation of the grid cell during that period relative to the regional means. The regression for grid cells that experienced 0-1 mortality events is: -0.007(Pr-Prregional) - 1.22 ($p<0.001$, $R^2 = 0.43$); the regression for sites that experienced greater than one mortality event is: -0.008(Pr-Prregional) + 1.70 ($p<0.001$, $R^2 = 0.20$). The dashed lines indicate the mean T-Tregional (1.95 ºC) and mean Pr-Prregional (-31.7mm) for the sites that experienced greater than one mortality event.

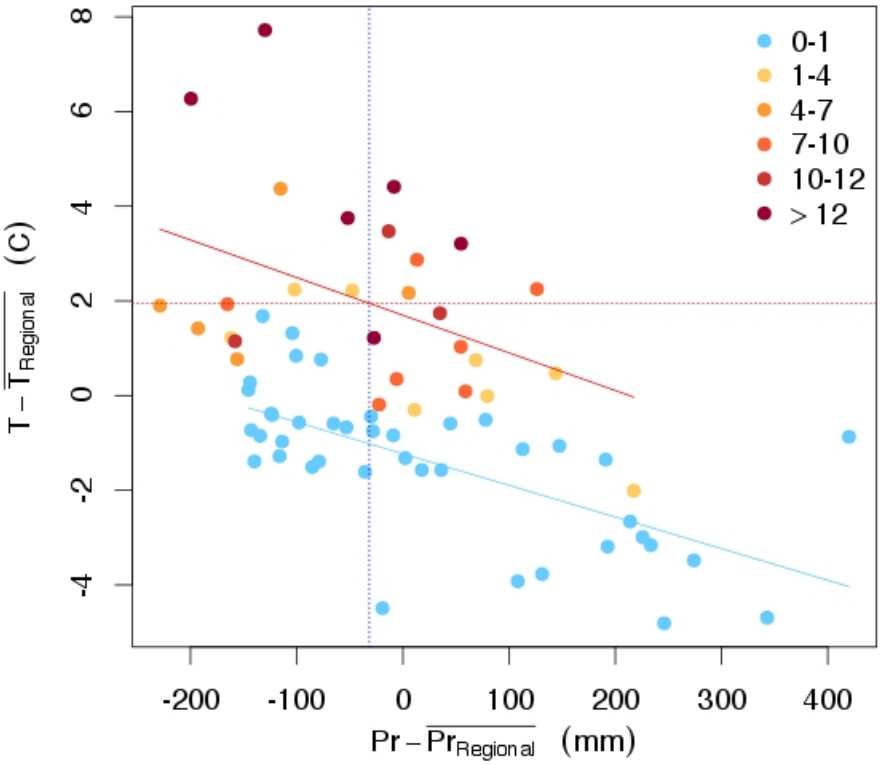

SI 9: Figure 4a-c. CMIP5 DGVM results: The changes in NET cover were calculated from three CMIP5 models that include dynamic vegetation distributions: HadGEM2-ES [TRIFFID DGVM (Cox, 2001), MIROC-ESM [SEIB-DGVM (Sato et al, 2007)], and MPI-ESM (Reick et al., 2013) models. Models are from the RCP8.5 scenario and include the percentage change in the PFT corresponding most closely to NET for each model: Needleleaf Trees (HadGEM2), Boreal Evergreen (MIROC), and Extra-tropical Evergreen Trees (MPI-ESM). Each of these models treats vegetation distributional dynamics differently: HadGEM2 uses a Lotka-Volterra approach to parameterize competition by PFTs for space and light (Cox, 2001); MIROC-ESM uses an individual-based model that considers spatially-explicit competition by PFTs for resources as well as bioclimatic limits on PFT growth (Sato et al, 2007); MPI-ESM simulates competition based on NPP (Reick et al., 2013).

There are two ways to calculate the loss and gain of NET in Figures 4A-C: (1) the total area that is gaining (blue color) and losing (red color) NET, or (2) the total area that lost and gained NET, i.e. the integral of the percentage lost and gained.

For method (1):
HadGEM2_ES lost 17.8 million km^2 and gained 20.3 million km^2;
MIROC_ESM lost 11.9 million km^2 and gained 19.4 million km^2;
MPI_ESM_MR lost 14.0 million km^2 and gained 31.8 million km^2.

For method (2),
HadGEM2_ES lost 1.88 million km^2 and gained 1.52 million km^2;
MIROC_ESM lost 2.09 million km^2 and gained 3.47 million km^2;
MPI_ESM_MR lost 0.70 million km^2 and gained 4.25 million km^2.

Figure 4d. Our simulations used the atmosphere (CAM, the Community Atmosphere Model) and land surface components (CLM, the Community Land Surface Model) of the Community Earth System Model (CESM). For the atmosphere, we employed the finite volume (FV) dynamical core and CAM version 4 physics with 26 vertical levels (Neale et al. 2010). The spatial resolution of the model is 1.9° latitude by 2.5° longitude. Exchanges of heat, moisture, and momentum fluxes between the land and the atmosphere are simulated by the land surface model, CLM, version 4.0. In CLM4.0, vegetation coverage is described in each grid cell by fractional areas of plant functional types (PFTs). There are 17 PFTs including bare ground, 11 tree PFTs, three grass PFTs, and two crop PFTs. CLM4.0 includes a carbon-nitrogen (CN) biogeochemical model that predicts vegetation, litter, soil carbon and nitrogen states, and vegetation phenology (Thornton *et al.* 2007). The dynamic vegetation is based on the Lund-Potsdam-Jena (LPJ) model (Sitch *et al.* 2003), wherein vegetation change is represented by a change in the fractional PFT coverage of a grid cell at the end of each year (Sitch *et al.* 2003). The LPJ dynamic component in CLM4.0 is among the most mechanistic of the existing DGVMs (McDowell *et al.* 2011). Plant functional types can change according to twenty-year climate envelopes based on temperature and precipitation limits as well as due to mortality mechanisms. Mortality can occur due to heat stress (based on an accumulation of growing degree days), fire, and growth efficiency. In our simulations, the interaction between the land and atmosphere components is two-way, unlike previous studies performed to evaluate the basic performance of CLM in CESM (*e.g.*, Gotangco Castillo *et al.* 2012).

The sea surface temperature data used as boundary conditions include results from simulations of 21st century climate under a medium-high emissions range (Special Report on Emissions Scenarios A1B, (Nakicenovic *et al.* 2000)). Output from the following eight models in the Coupled Model Intercomparison Project version 3 (CMIP3) (Meehl *et al.* 2007) were used: the National Center for Atmospheric Research Community Climate Model, version 3 (NCAR-CCSM3); Météo-France / Centre National de Recherches Météorologiques Coupled Global Climate Model, version3 (CNRM-CM3); Max Planck Institute for Meteorology ECHAM5 (MPI-ECHAM5); Geophysical Fluid Dynamics Laboratory Climate Model version 2.1 (GFDL-CM2-1); Goddard Institute for Space Studies Model R, coupled with Russell ocean component (GISS-ER); Hadley Centre Coupled Model, version 3 (UKMO-HadCM3); Hadley Centre Met Office Hadley Centre Global Environmental Model, version 1 (UKMO-HadGEM1); and Meteorological Research Institute Coupled Atmosphere- Ocean General Circulation Model, version 2.3.2 a (MRI-CGCM2.3A).The CESM simulations employed here proved accurate for simulating the current vegetation coverage in North America (Jiang et al. 2013).

Cox, P. M. Description of the TRIFFID dynamic global vegetation model, *Hadley Centre Technical note*, *24* (2001).

Gotangco Castillo, C. K., S. Levis, and P. Thornton, Evaluation of the new CNDV option of the Community Land Model: Effects of dynamic vegetation and interactive nitrogen on CLM4 means and variability. *J. Climate*, **25**, 3702–3714. (2012)

McDowell, N.G., D. Beerling, D. Breshears, R. Fisher, K. Raffa, M. Stitt. Interdependence of mechanisms underlying climate-driven vegetation mortality. *Trends in Ecology and Evolution*, **26,** 523-532. (2011)

Meehl, G. A., C. Covey, K. E. Taylor, T. Delworth, R. J. Stouffer, M. Latif, B. McAvaney, J. F. B. Mitchell, The WCRP CMIP3 multimodel dataset: A new era in climate change research. *Bull. Amer. Meteor. Soc.*, **88**, 1383–1394. (2007)

Nakićenović, N., *et al*, Special Report on Emissions Scenarios. Cambridge University Press, 570 pp. (2000)

Neale, R. B., et al, Description of the NCAR Community Atmosphere Model (CAM 4.0). NCAR Tech. Note NCAR/TN-485+STR, 212 pp. [Available online at http://www.cesm.ucar.edu/models/ccsm4.0/cam/docs/description/cam4_desc.pdf.] (2010)

Reick, C. H., T. Raddatz, V. Brovkin, and V. Gayler, Representation of natural and anthropogenic land cover change in MPI-ESM, *Journal of Advances in Modeling Earth Systems*, **5**(3), 459-482. (2013)

Sato, H., A. Itoh, and T. Kohyama, SEIB–DGVM: A new Dynamic Global Vegetation Model using a spatially explicit individual-based approach, *Ecological Modelling*, **200**(3–4), 279-307. (2007)

Sitch, S., *et al*., Evaluation of ecosystem dynamics, plant geography and terrestrial carbon cycling in the LPJ dynamic global vegetation model. *Global Change Biol*., **9**, 161–185. (2003)

Thornton, P. E., J. F. Lamarque, N. A. Rosenbloom, and N. M. Mahowald, Influence of carbon-nitrogen cycle coupling on land model response to CO_2 fertilization and climate variability. *Global Biogeochem. Cycles, 21*, GB4018, doi:10.1029/2006GB002868. (2007)